

Machine-learning classification with additivity and diverse multifractal pathways in multiplicativityMadhur Mangalam^{1,*}, Henrik Seckler^{2,†} and Damian G. Kelty-Stephen^{3,‡}¹*Division of Biomechanics and Research Development, Department of Biomechanics, and Center for Research in Human Movement Variability, University of Nebraska at Omaha, Omaha, Nebraska 68182, USA*²*Institute for Physics & Astronomy, University of Potsdam, Potsdam-Golm 14476, Germany*³*Department of Psychology, State University of New York at New Paltz, New Paltz, New York 12561, USA*

(Received 6 May 2024; accepted 2 August 2024; published 10 September 2024)

Evidence of multifractal structures has spread to a wider set of physiological time series supporting the intricate interplay of biological and psychological functioning. These dynamics manifest as random multiplicative cascades, embodying nonlinear relationships characterized by recurring division, branching, and aggregation processes implicating noise across successive generations. This investigation focuses on how well the diversity of multifractal properties can be specific to the type of cascade relationship between generation (i.e., multiplicative, additive, or a mixture) as well as to the type of noise (i.e., including additive white Gaussian noise, fractional Gaussian noise, and various amalgamations) among 15 distinct types of binomial cascade processes. Cross-correlation analysis of multifractal spectral features confirms that these features capture nuanced aspects of cascading processes with minimal redundancy. Principal component analysis using 13 distinct multifractal spectral features shows that different cascade processes can manifest multifractal evidence of nonlinearity for distinct reasons. This transparency of multifractal spectral features to underlying cascade dynamics becomes less amenable to machine-learning strategies. Fully connected neural networks struggled to classify the 15 distinct types of cascade processes based on the respective multifractal spectral features (45.5% accuracy) yet demonstrated improved accuracy when addressing single categories of cross-generation relationships, that is, additive (91.6%), multiplicative (75.4%), or additomultiplicative (70.6%). While traditional principal component analysis reveals distinct loadings attributed to individual noise processes, multiplicative relationships between generations effectively make the constituent noise processes less discernible to neural networks. Neural networks may lack sufficient hierarchical depth required to effectively distinguish among nonadditive cascading processes, recommending either elaborating multifractal geometry or using alternate architectures for machine-learning classification of cascades with multiplicative relationships.

DOI: [10.1103/PhysRevResearch.6.033276](https://doi.org/10.1103/PhysRevResearch.6.033276)**I. INTRODUCTION**

Machine-learning models have become increasingly prevalent across applications, tackling complex problems and optimization processes in domains ranging from healthcare and finance to manufacturing and beyond [1–5]. This trend is driven by results that may elude traditional analytical approaches. Researchers across disciplines have increasingly begun to leverage machine learning’s capacity to uncover patterns, correlations, and insights from vast datasets towards analyzing experimental data, predict outcomes, and gain deeper insights into the underlying mechanisms governing natural phenomena [6–9]. Integrating machine-learning algorithms with physics-based modeling holds immense promise

in elucidating the generative mechanisms that govern the observed behavior of study processes within various scientific domains. Incorporating machine-learning algorithms with physics-based modeling promises to help identify, characterize, and understand complex systems and processes [10–15], allowing extraction of data-driven insights that can refine theoretical models and advance our understanding of the complexity of the natural world [16].

While machine-learning methodologies aim to advance our understanding of complex systems generating health and disease [17–19], they are not without limitations. The reliance on large datasets for training machine-learning models can be prohibitive, especially in fields where data collection is costly or time consuming. Then again, even with an extensive training data set, the impeccable performance of machine-learning models within a single dataset is no guarantee that the same model’s performance on independent data sets will not regress to chance levels [20,21]. Successful classification is then only half of the scientific battle. The subsequent hurdle is the interpretability of machine-learning models, particularly in complex biological and psychological systems where the underlying processes may be poorly understood. Machine-learning models often operate as “black boxes,” making it

*Contact author: mmangalam@unomaha.edu†Contact author: hseckler@uni-potsdam.de‡Contact author: keltystd@newpaltz.edu

difficult to discern how they arrive at their predictions or classifications [22–24]. Biological and psychological systems constitute thickets of interacting variables and processes across multiple scales, and the solution of a “black box” may serve well for prediction but offer little new explanatory clarity.

Therefore, the promise of machine learning for advancing basic scientific research in these areas will depend on the strategic choice of features that address the known theoretical roots of observed complexity in the measured record. Biology and psychology have begun to view adaptive functioning through the theoretical formalism of “cascades” embodying nonlinear interactions across nested spatial and temporal scales [25–27]. While linear modeling with normal (Gaussian) patterns of residual variability suits systems with numerous modular components exhibiting ergodicity, biological and psychological functions break ergodicity and display nonlinear temporal correlations across multiple scales, consistent with cascading dynamics generating non-normal (non-Gaussian) distributions, such as power laws with scale-invariant tails [28–39]. The scale-invariant patterns render a linear model’s traditional first and second moments inadequate or unstable for characterizing the cascade processes. Instead, characterizing cascades requires multifractal geometry. Although a single power law tail entails “fractal” or “monofractal” systems, cascade-like interactions across multiple scales give rise to ergodicity-breaking processes exhibiting by multiple power laws, warranting the term “multifractal” [40,41]. Multifractal analysis allows addressing differently sized events in heterogeneous time series using a q parameter emphasizing progressively smaller or larger events for $q < 0$ and $q > 0$, respectively. Each value of q allows estimating power laws describing the growth of the “proportion” of magnitude and “Shannon entropy” over progressively larger timescales, yielding power-law exponents $\alpha(q)$ and $f(q)$, respectively [42]. The set of $\alpha(q)$ and $f(q)$ definable for the measurement time series over many values of q follow an asymmetric, inverted-“U” called the multifractal spectrum [43]. Positive, zero, and negative q values allow the definition of the left side, peak, and right side of the multifractal spectrum. Whereas the observed cascade-like behavior in raw form is ergodicity breaking, simulation work has shown that features of the multifractal spectrum can differ according to the type of the constituent stochastic process [44–46], and multifractal descriptors are themselves ergodic and amenable to linear cause-and-effect models [47–51]. Multifractal descriptors are, therefore, apt operationalizations of how cascades may underpin adaptive biological and psychological functioning, and they offer a good first step towards classifying noncascade diffusion models [52].

Should cascades facilitate adaptive organismal functioning, science stands to gain from the characterization of underlying cascade structures through the multifractal properties of measured functioning. The multifractal evidence of cascade-like nonlinear interactions across scales consistently supports statistical predictions of adaptive behaviors across various domains: postural control [53–56], brain function [57,58], cognition [59–61], and perceptuomotor responses [62–68]. Multifractal geometry also helps explain ergodicity-breaking and adaptive aspects of measured biological and

psychological behavior [47–51]. Multifractal structure of bodywide movement fluctuations and linear causal models confirm that perceptuomotor performance depends on a bodywide network of multifractal flows [69–71]. In a practical context, understanding these multifractal fluctuations may aid in detecting disorders [72,73] and providing noninvasive but targeted interventions to support accurate perceptual performance [74–77]. Examples abound in physiology with multifractal structure supporting these ambitions: multifractality has been shown to discriminate cognitive performance using electroencephalography (EEG) signals [78,79], age-related changes in the peripheral cardiovascular system through laser Doppler flowmetry (LDF) signals [80,81], Parkinson’s and Huntington’s diseases based on stride intervals [82,83], Parkinson’s disease through postural center of pressure (CoP) fluctuations [84], arrhythmia detection [85], chronic heart disease diagnosis [86], congestive heart failure assessment [87,88], and fibromyalgia evaluation [89] using electrocardiogram (EKG) signals. Additionally, multifractal analysis has shown promise in identifying migraine patterns based on cerebral blood flow [81], amyotrophic lateral sclerosis (ALS) symptoms using electromyography (EMG) signals [90], Alzheimer’s disease diagnosis through EEG signals [91], detection of driving fatigue via EEG signals [92], and identification of metastatic bone disease from microscopic images [93]. Multifractal geometries are not just theoretically consonant with the role of multiplicative interactions that drive cascades but are empirically effective as predictors in standard regression models of adaptive organismal functioning.

Indeed, multifractal spectral features have proven their efficacy in supporting machine learning across various domains, from physiology to perception, action, and cognition. For example, the incorporation of multifractal features into machine-learning algorithms has enabled the discrimination between healthy, interictal, and seizure activities [94], automatic seizure [95–97] and intention [98] detection using EEG signals, early detection of diabetic retinopathy using macular images [99,100], Alzheimer’s disease diagnosis via functional magnetic resonance imaging (fMRI) images [101–103], texture discrimination of hepatocellular carcinoma in histopathological images [104], fatigue assessment using EMG signals [105,106], glioma detection in brain MRI scans [107], and classification of breast cancer from ultrasound images [108]. Thus, ample evidence suggests that multifractal features could enhance the ability of machine-learning models to detect the rich texture of cascade-like nonlinear interactions across scales. Multifractal features have also supplemented machine learning in understanding what constitutes “good” arts and music. Multifractal features offer the capability to discern the textural regularities present in paintings by Vincent van Gogh across different periods and differentiate between van Gogh’s works and those of his contemporaries [109]. The multifractal analysis offers intriguing insights into music’s melodic and rhythmic dimensions, both in humans and birds [110–112]; in humans, specifically distinguishing various styles of music based on the shape and opening width of the multifractal spectrum. Furthermore, emotional nuances like happiness, sadness, calmness, and anxiety within Indian classical music can be discerned to comparable extents using both machine-learning models and multifractal

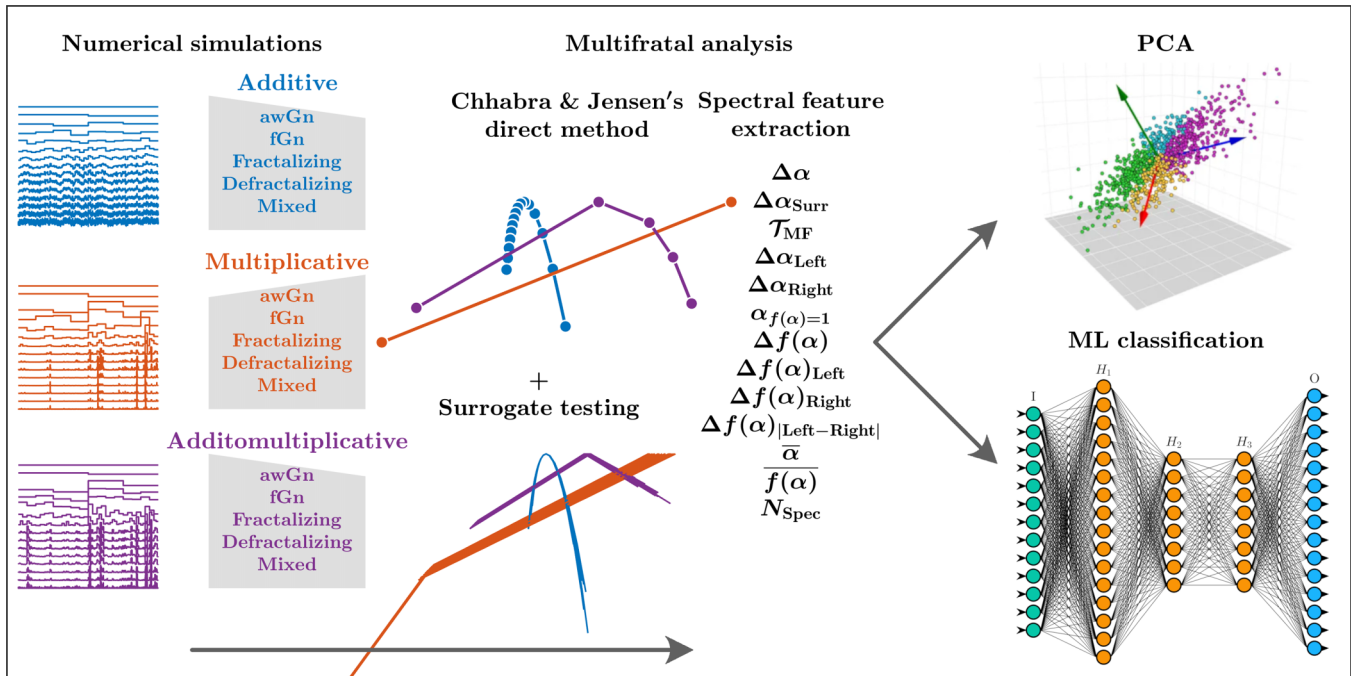


FIG. 1. Schematic of the present study.

characteristics [113], and incorporating multifractal descriptors into machine-learning models shows promise in enhancing the classification accuracy of music performers [114].

All of the foregoing examples offer intriguing examples of how multifractal properties might be useful for classifying overt properties of adaptive function; that is, we could confirm these classifications with an eventual assay or biopsy or with a direct question to a verbal human. Successful machine-learning discrimination can thus often focus on extreme cases with clear benchmarks for success. For example, when identifying patients with Parkinson's disease, the analysis typically involves two pre-labeled groups, healthy adults and those with Parkinson's disease, resulting in high discrimination accuracy (e.g., [115–118]). However, an open question is how to develop machine learning to discern what we cannot later confirm straightforwardly. For instance, real-world scenarios present diverse patient pools exhibiting Parkinsonism to varying degrees or Parkinsonism-like manifestations of non-Parkinson's origins [119–121]. The deep structure of potential cascading dynamics may be diagnostically ambiguous and cluttered by overlapping symptoms or measurement errors. In such conditions, and generally as well, it is crucial for machine-learning models to identify the underlying generative processes leading to emergent multifractal structure. This is because the multifractal structure may encompass a variety of interacting processes in various ways, which can be obscured beneath it [44–46]. Knowing exactly how a resulting cascade process arose will be rare outside of numerical simulation. However, it would be both scientifically interesting and clinically insightful if machine-learning strategies could capitalize upon the relationship between multifractal features and the cascade-like generating mechanism, which may not map singly to any local anatomical part or single specific tissue, for example, a tumor [122]. Whether current machine-learning models can analytically discern various sources

contributing to nonlinear interactions across scales remains uncertain. This uncertainty is significant because the potential insights of multifractal features would be limited without the ability to discriminate between the nuances of generative mechanisms. Ultimately, we are curious whether machine learning could transform multifractal features from intriguing downstream consequences of possible cascade dynamics into effective detection/prediction of latent or ambiguous physical processes.

The paper is organized as follows: We conducted numerical simulations of 15 types of binomial cascade processes generated by a spectrum of noise processes. These include additive white Gaussian noise (awGn), fractional Gaussian noise (fGn), and various amalgamations (Fig. 1). These processes demonstrate additive and multiplicative interactions, with a stochastic combination of the two interaction types occurring across constituent noise processes at different scales. We used multifractal analysis to estimate a wide range of multifractal-spectral features for the simulated cascade time series to multifractal analysis. Subsequently, we used cross-correlation analysis on these features to investigate whether they capture specific or nuanced aspects of the multifractal structure. We used principal component analysis (PCA) across these multifractal spectral features to discern whether and how these features contribute to multifractal signatures of nonlinearity in each cascade type above and beyond the cascades' linear features. Finally, we deployed fully connected neural networks to classify the 15 distinct cascade processes based on multifractal spectral features. We anticipated observing variations across cascade types in cross-correlation and PCA results, indicative of multiple pathways leading to emergent multifractal structure. Moreover, we hypothesized that if neural networks could delineate the hierarchical structure of multiplicative cascades, they should be capable of discriminating between these cascade processes.

II. METHODS

A. Generating random cascade series

1. Prior cascade simulation using binomial fracturing and applying binomial noise

Cascade processes manipulate n_g cells successively over g generations distributing the proportion $p_{i,j}$ that each i th parent cell in generation j (for $j < g$, $i \leq n_j$) bequeaths to n_c children cells in generation $j+1$ each carrying $p_{k,j+1}$, for $i \leq k \leq n_{j+1}$. We produced 15 types of random binomial cascades as described below across multiple combinations of the constituent noise and cross-generation relationships. Cascades are “binomial” when two children cells inherit the proportion from each parent cell from the prior generation (i.e., $n_c = 2$). Cascades are multiplicative or additive when the n_c children-cell proportions reflect n_c different multiplications or additions, respectively, governing the distribution of the parent cell’s proportion. These cascades produce children cells by binomially fracturing the parent cells from generation to generation. In this framework, binomial noise terms might match the children cells (Fig. 2). For every i th parent cell in generation j , binomial noise terms could be deterministic, for example, applying the same noise terms $W_1 = 0.25$ and $W_2 = 0.75$ to calculate the proportions in the $(2i-1)$ th and the $2i$ th children cells in the $(j+1)$ th generation as $p_{2i-1,j+1} = p_{i,j}W_1$ and $p_{2i,j+1} = p_{i,j}W_2$, respectively.

2. Beyond binomial noise terms: Random binomial-fracturing cascades with noise terms defined across entire generations to test for effects of additivity and multiplicativity

We used numerical simulations of random cascades to approximate the heterogeneity of random component processes and measured outcomes frequently appearing in biological and psychological measurements. This work preserved the traditional binomial fracturing across successive generations to maintain the same rate of lengthening the cascading time series. However, whereas traditional binomial cascade modeling often repeats the same set of weights W_1 and W_2 separately for each i th parent [48], we generated the cascade series using noise terms defined across the entire generation, either as awGn, fGn, or progressively stronger or weaker temporal correlations in awGn and fGn, respectively. So, we defined the noise term $W_{t,j+1}$, $t = 1, 2, \dots, n_{j+1}$ as a Gaussian distribution with $\mu = 1$ and $\sigma = 1$ with linear correlation of noise terms in fGn from $t = 1, 2, \dots, n_{j+1}$ determined by H_{fGn} which was 0.5 or 1 for ideal awGn or ideal fGn, respectively.

(1) *Additive awGn cascades.* Noise terms for generation $j+1$ follow $W_{t,j+1} = awGn$, $\mu = 1$, $\sigma = 1$ (where μ is mean and σ is standard deviation), and the $(2i-1)$ th and $2i$ th children cells in the $(j+1)$ th generation hold proportions $p_i + W_{2i-1,j+1}$ and $p_i + W_{2i,j+1}$, respectively.

(2) *Additive fGn cascades.* Noise terms for generation $j+1$ follow $W_{t,j+1} = fGn$, $\mu = 1$, $\sigma = 1$, $H_{fGn} = 1$, and the $(2i-1)$ th and $2i$ th children cells in the $(j+1)$ th generation hold proportions $p_i + W_{2i-1,j+1}$ and $p_i + W_{2i,j+1}$, respectively.

(3) *Additive fractalizing noise cascades.* Noise terms for generation $j+1$ follow $W_{t,j+1} = fGn$, $\mu = 1$,

$\sigma = 1$, $H_{fGn} = \frac{1}{14}(j+1)$, and the $(2i-1)$ th and $2i$ th children cells in the $(j+1)$ th generation hold proportions $p_i + W_{2i-1,j+1}$ and $p_i + W_{2i,j+1}$, respectively.

(4) *Additive defractalizing noise cascades.* Noise terms for generation $j+1$ follow $W_{t,j+1} = fGn$, $\mu = 1$, $\sigma = 1$, $H_{fGn} = 1 - \frac{1}{14}(j+1)$, and the $(2i-1)$ th and $2i$ th children cells in the $(j+1)$ th generation hold proportions $p_i + W_{2i-1,j+1}$ and $p_i + W_{2i,j+1}$, respectively.

(5) *Additive mixed noise cascades.* Noise terms for $j+1$ follow $W_{t,j+1} = fGn$, $\mu = 1$, $\sigma = 1$, $H_{fGn} = \begin{Bmatrix} 0.5 \\ 1 \end{Bmatrix}$, and the $(2i-1)$ th and $2i$ th children cells in the $(j+1)$ th generation hold proportions $p_i + W_{2i-1,j+1}$ and $p_i + W_{2i,j+1}$, respectively.

(6) *Multiplicative awGn cascades.* Noise terms for generation $j+1$ follow $W_{t,j+1} = awGn$, $\mu = 1$, $\sigma = 1$, and the $(2i-1)$ th and $2i$ th children cells in the $(j+1)$ th generation hold proportions $p_i W_{2i-1,j+1}$ and $p_i W_{2i,j+1}$, respectively.

(7) *Multiplicative fGn cascades.* Noise terms for generation $j+1$ follow $W_{t,j+1} = fGn$, $\mu = 1$, $\sigma = 1$, $H_{fGn} = 1$, and the $(2i-1)$ th and $2i$ th children cells in the $(j+1)$ th generation hold proportions $p_i W_{2i-1,j+1}$ and $p_i W_{2i,j+1}$, respectively.

(8) *Multiplicative fractalizing noise cascades.* Noise terms for generation $j+1$ follow $W_{t,j+1} = fGn$, $\mu = 1$, $\sigma = 1$, $H_{fGn} = \frac{1}{14}(j+1)$, and the $(2i-1)$ th and $2i$ th children cells in the $(j+1)$ th generation hold proportions $p_i W_{2i-1,j+1}$ and $p_i W_{2i,j+1}$, respectively.

(9) *Multiplicative defractalizing noise cascades.* Noise terms for generation $j+1$ follow $W_{t,j+1} = fGn$, $\mu = 1$, $\sigma = 1$, $H_{fGn} = 1 - \frac{1}{14}(j+1)$, and the $(2i-1)$ th and $2i$ th children cells in the $(j+1)$ th generation hold proportions $p_i W_{2i-1,j+1}$ and $p_i W_{2i,j+1}$, respectively.

(10) *Multiplicative mixed noise cascades.* Noise terms for $j+1$ follow $W_{t,j+1} = fGn$, $\mu = 1$, $\sigma = 1$, $H_{fGn} = \begin{Bmatrix} 0.5 \\ 1 \end{Bmatrix}$, and the $(2i-1)$ th and $2i$ th children cells in the $(j+1)$ th generation hold proportions $p_i W_{2i-1,j+1}$ and $p_i W_{2i,j+1}$, respectively.

(11) *Additomultiplicative awGn cascades.* Noise terms for generation $j+1$ follow $W_{t,j+1} = awGn$, $\mu = 1$, $\sigma = 1$, and the $(2i-1)$ th and $2i$ th children cells in the $(j+1)$ th generation hold proportions $p_i \Theta W_{2i-1,j+1}$ and $p_i \Theta W_{2i,j+1}$, respectively, with $\Theta = \begin{Bmatrix} + \\ \times \end{Bmatrix}$.

(12) *Additomultiplicative fGn cascades.* Noise terms for generation $j+1$ follow $W_{t,j+1} = fGn$, $\mu = 1$, $\sigma = 1$, $H_{fGn} = 1$, and the $(2i-1)$ th and $2i$ th children cells in the $(j+1)$ th generation hold proportions $p_i \Theta W_{2i-1,j+1}$ and $p_i \Theta W_{2i,j+1}$, respectively, with $\Theta = \begin{Bmatrix} + \\ \times \end{Bmatrix}$.

(13) *Additomultiplicative fractalizing noise cascades.* Noise terms for generation $j+1$ follow $W_{t,j+1} = fGn$, $\mu = 1$, $\sigma = 1$, $H_{fGn} = \frac{1}{14}(j+1)$, and the $(2i-1)$ th and $2i$ th children cells in the $(j+1)$ th generation hold proportions $p_i \Theta W_{2i-1,j+1}$ and $p_i \Theta W_{2i,j+1}$, respectively, with $\Theta = \begin{Bmatrix} + \\ \times \end{Bmatrix}$.

(14) *Additomultiplicative defractalizing noise cascades.* Noise terms for generation $j+1$ follow $W_{t,j+1} = fGn$, $\mu = 1$, $\sigma = 1$, $H_{fGn} = 1 - \frac{1}{14}(j+1)$, and the $(2i-1)$ th and $2i$ th children cells in the $(j+1)$ th generation hold proportions $p_i \Theta W_{2i-1,j+1}$ and $p_i \Theta W_{2i,j+1}$, respectively, with $\Theta = \begin{Bmatrix} + \\ \times \end{Bmatrix}$.

(15) *Additomultiplicative mixed noise cascades.* Noise terms for $j+1$ follow $W_{t,j+1} = fGn$, $\mu = 1$, $\sigma = 1$, $H_{fGn} = \begin{Bmatrix} 0.5 \\ 1 \end{Bmatrix}$, and the $(2i-1)$ th and $2i$ th children cells in the $(j+1)$ th

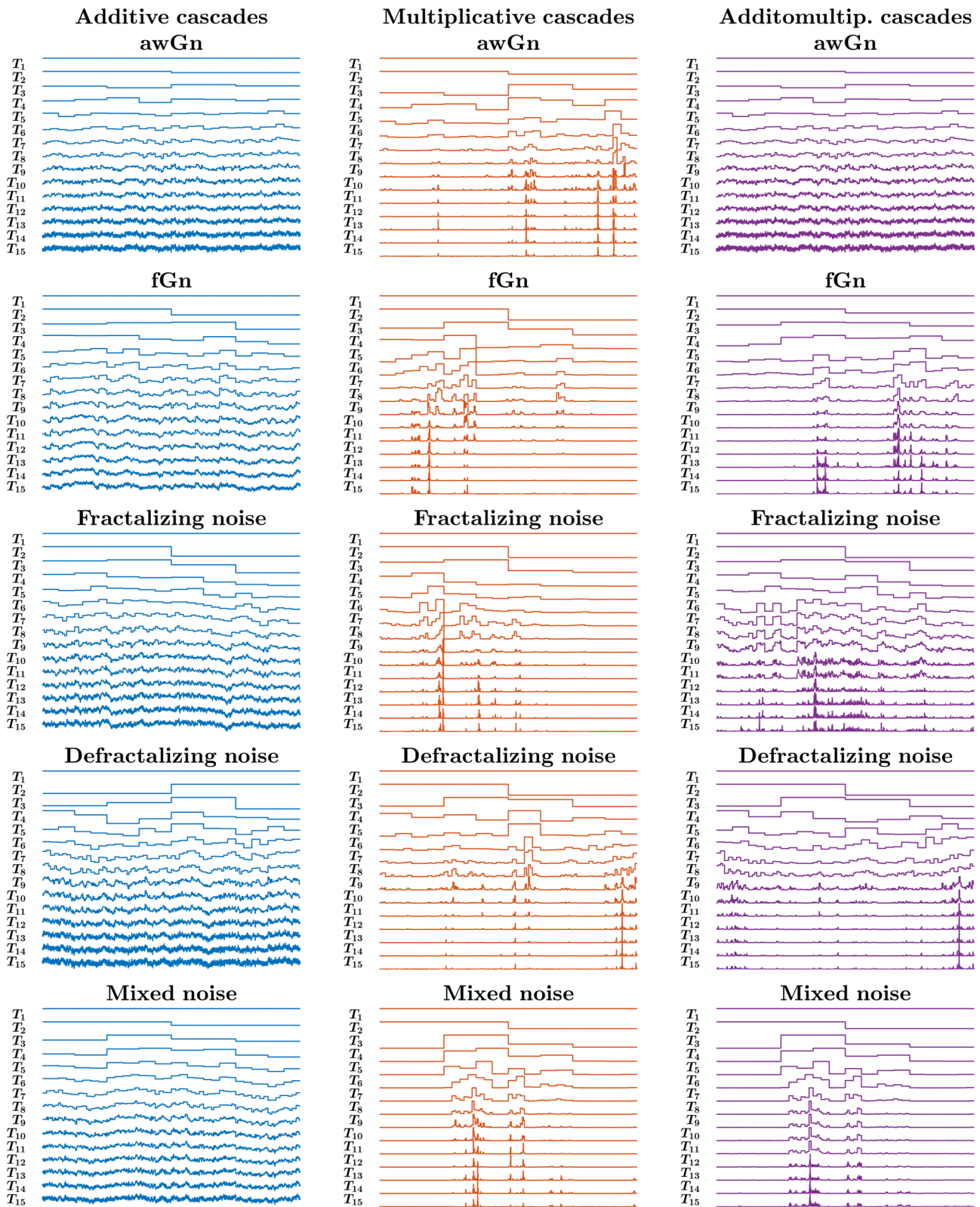


FIG. 2. Cascades provide a mathematical framework for understanding how complex distributions arise from iteratively subdividing and perturbing probability mass with noise across finer timescales. In the *left* and *center* panels, we observe random additive and multiplicative cascades implementing various noise terms through addition and multiplication across 15 successive generations. The *right* panel showcases a cascade with an admixture of additivity and multiplicative interactions. For clarity, we have normalized the data by maxima and vertically spaced them by a unit.

generation hold proportions $p_i \ominus W_{2i-1,j+1}$ and $p_i \ominus W_{2i,j+1}$, respectively, with $\ominus = \{ \times^+ \}$.

We simulated cascades comprising $2^{14} = 16384$ samples in the fifteenth and ultimate generation, aiming to elucidate the underlying factors contributing to multifractal patterns in biology and psychology. We generated a 100 cascading time series for cross-correlation and principal component analyses for each type. Regarding machine-learning models, we simulated 10 000 cascading time series for each type, with 98% allocated to the training set and 2% to the validation and the testing set.

B. Multifractal analysis

1. Assessing multifractal nonlinearity using the direct-estimation of singularity spectrum

We used Chhabra and Jensen's [42] direct method for all analyses. This method estimates multifractal spectrum width $\Delta\alpha$ by sampling a series $x(t)$ at progressively larger scales using the proportion of signal $P_i(n)$ falling within the v th bin of scale n as

$$P_v(n) = \frac{\sum_{k=(v-1)n+1}^{v \cdot n} x(k)}{\sum x(t)}, \quad n = \{4, 8, 16, \dots\} < T/8. \quad (1)$$

As n increases, $P_v(n)$ represents a progressively larger proportion of $x(t)$,

$$P(n) \propto n^\alpha, \quad (2)$$

suggesting a growth of the proportion according to one "singularity" strength α [123]. $P(n)$ exhibits multifractal dynamics when it grows heterogeneously across time scales n according to multiple singularity strengths, such that

$$P(n_v) \propto n^{\alpha_v}, \quad (3)$$

whereby each v th bin may show a distinct relationship of $P(n)$ with n . The width of this singularity spectrum, $\Delta\alpha = (\alpha_{\max} - \alpha_{\min})$, indicates the heterogeneity of these relationships [43,124].

Chhabra and Jensen's [42] method estimates $P(n)$ for N_n nonoverlapping bins of n sizes and transforms them into a "mass" $\mu(q)$ using a q parameter emphasizing higher or lower $P(n)$ for $q > 1$ and $q < 1$, respectively, in the form

$$\mu_v(q, n) = \frac{[P_v(n)]^q}{\sum_{j=1}^{N_n} [P_j(n)]^q}. \quad (4)$$

Then, $\alpha(q)$ is the singularity for mass μ -weighted $P(n)$ estimated as

$$\begin{aligned} \alpha(q) &= - \lim_{N_n \rightarrow \infty} \frac{1}{\ln N_n} \sum_{v=1}^{N_n} \mu_v(q, n) \ln P_v(n) \\ &= \lim_{n \rightarrow 0} \frac{1}{\ln n} \sum_{v=1}^{N_n} \mu_v(q, n) \ln P_v(n). \end{aligned} \quad (5)$$

Each estimated value of $\alpha(q)$ belongs to the multifractal spectrum only when the Shannon entropy of $\mu(q, n)$ scales with n

according to the Hausdorff dimension $f(q)$ [42], where

$$\begin{aligned} f(q) &= - \lim_{N_n \rightarrow \infty} \frac{1}{\ln N_n} \sum_{v=1}^{N_n} \mu_v(q, n) \ln \mu_v(q, n) \\ &= \lim_{v \rightarrow 0} \frac{1}{\ln n} \sum_{v=1}^{N_n} \mu_v(q, n) \ln \mu_v(q, n). \end{aligned} \quad (6)$$

For values of q yielding a strong relationship between Eqs. (5) and (6)—in this study, correlation coefficient $r > 0.95$ —the parametric curve $(\alpha(q), f(q))$ or $(\alpha, f(\alpha))$ constitutes the multifractal spectrum and $\Delta\alpha$ (i.e., $\alpha_{\max} - \alpha_{\min}$) constitutes the multifractal spectrum width. r determines that only scaling relationships of comparable strength can support the estimation of the multifractal spectrum, whether generated as cascades or surrogates. Using a correlation benchmark aims to operationalize previously raised concerns about mis-specifications of the multifractal spectrum [125].

2. Calculating \mathcal{T}_{MF} based on comparison with iterated amplitude adjusted Fourier transform (IAAFT) surrogates

We employed the iterated amplitude adjusted Fourier transform (IAAFT) to derive t_{MF} . The goal was to ascertain whether nonzero $\Delta\alpha$ values were indicative of multifractality stemming from nonlinear interactions across various timescales. We compared $\Delta\alpha$ between the original time series and a set of 32 IAAFT surrogates [126,127]. The IAAFT technique symmetrical rearranges the original values around the autoregressive structure, generating surrogates that randomize the phase ordering of the spectral amplitudes in the series while preserving linear temporal correlations. We computed the one-sample t -statistic, denoted as t_{MF} , by calculating the difference between $\Delta\alpha$ for the original series and the same for the 32 surrogates, divided by the standard error of the spectrum width for the surrogates.

3. Multifractal spectral features

Multifractal spectra manifest as intricate functions, displaying diverse widths and heights throughout their two-dimensional domain. They showcase asymmetry and irregular spacing across different parameter ranges q , denoting variability in the heterogeneity of fluctuations. To comprehensively capture the nuanced facets of multifractal spectra, we integrated a diverse array of features, encompassing a broad spectrum of characteristics for each cascade time series, as depicted in Fig. 3 and Table I.

C. Principal component analysis (PCA)

Principal component analysis (PCA) is a statistical technique for dimensionality reduction; we employed PCA to identify the underlying patterns and reduce the dimensionality of our dataset. This method extracts a set of linearly uncorrelated variables, called principal components, from the original multifractal spectral features. These components capture the maximum variance in the data while minimizing information loss. In MATLAB (Mathworks Inc., Natick, MA), PCA analysis was conducted using built-in functions, enabling efficient computation and visualization of the results. We conducted PCA on the correlation matrix comprising the 13 multifractal spectral features separately for each of the 15 cascade types.

TABLE I. Multifractal spectral features.

Features
Multifractal spectral width of the original time series, $\Delta\alpha$
Multifractal spectral width of the IAAFT surrogate time series, $\Delta\alpha_{\text{Surr}}$
Multifractal nonlinearity, \mathcal{T}_{MF}
Left-side width of the original spectrum, $\Delta\alpha_{\text{Left}}$
Right-side width of the original spectrum, $\Delta\alpha_{\text{Right}}$
Horizontal location of the singularity, $\alpha_{f(\alpha)=1}$
Height of the original spectrum, $\Delta f(\alpha)$
Left-side height of the original spectrum, $\Delta f(\alpha)_{\text{Left}}$
Right-side height of the original spectrum, $\Delta f(\alpha)_{\text{Right}}$
Difference in the left- and right-side height of the original spectrum, $\Delta f(\alpha)_{ \text{Left}-\text{Right} }$
Mean of α values, $\bar{\alpha}$
Mean of $f(\alpha)$ values, $\overline{f(\alpha)}$
Number of points in the original spectrum, N_{Spec}

Utilizing the correlation matrix—as opposed to using the covariance matrix—entails standardizing each variable to have a mean of 0 and a standard deviation of 1, effectively addressing the challenge posed by the varying magnitude scales of different features [128]. Finally, to visually depict the similarity among principal components, we employed Lloyd’s algorithm [129] for k -means clustering, partitioning the principal components into four distinct clusters.

D. Machine-learning classifiers

A neural network can be likened to an intricate function approximator, striving to synchronize its outputs, $f_{\theta}(X_i)$, with

the true target values, \hat{Y}_i , based on the corresponding input data X_i [130,131]. A neural network consists of multiple layers of interconnected neurons at its core. Within each layer, the output value of a neuron denoted as $O_{k,l}$ in layer l , is computed as the weighted sum of all neurons in the preceding layer, $O_{k,l-1}$, followed by passage through an activation function h :

$$O_{k,l} = h\left(\sum_k \theta_{k',k}^{(l)} O_{k,l-1} + \theta_{k',0}^{(l)}\right). \tag{7}$$

Here, $\theta_{k',k}^{(l)}$ represents the weight connecting neuron k' in the l th layer to neuron k in the $(l - 1)$ th layer, with $\theta_{k',0}^{(l)}$ serving as an additional offset. The output $f_{\theta}(X_i)$ of the neural network mirrors the values of the neurons in the final layer, while the input X_i reflects the values of the neurons in the initial layer.

The neural network’s weights, denoted collectively as θ , are determined by minimizing a loss function applied to a training dataset. Often, this loss function takes the form of the negative-log-likelihood loss [130]:

$$\mathcal{L}_{\text{nll}} = - \sum_i \log p(\hat{Y}_i | f_{\theta}(X_i)). \tag{8}$$

Here, $p(\hat{Y}_i | f_{\theta}(X_i))$ signifies the probability assigned by the neural network to the true target \hat{Y}_i given input X_i . In classification tasks, our objective typically involves predicting discrete probabilities, labeled as $p_{i,k}$, regarding each class k as the true label for input X_i . In this scenario, the negative-log-likelihood transforms into the widely recognized cross-entropy loss [132]:

$$\mathcal{L}_{\text{cel}} = - \sum_{i,k} \hat{Y}_{i,k} \log(p_{i,k}), \tag{9}$$

where $\hat{Y}_{i,k} = \delta_{jk}$ is a binary indicator of the true label j_i of input X_i .

This loss function is optimized by applying stochastic gradient descent [133]. This study employed an advanced variant of stochastic gradient descent called “adaptive moment estimation” (Adam) [134]. Additionally, we integrated “stochastic weight averaging Gaussian” (SWAG),

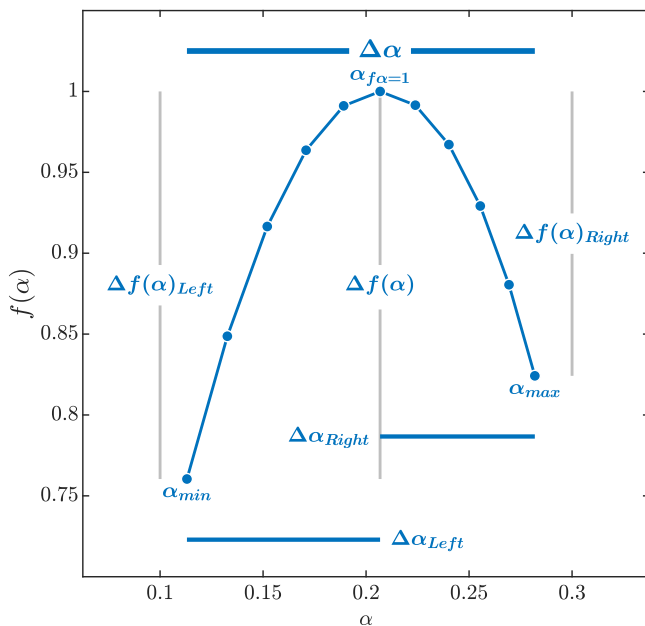


FIG. 3. Determining multifractal spectral features of cascade processes. The multifractal spectrum of each trajectory was created by plotting the parametric curve $\{\alpha(q), f(q)\}$. $\alpha(q)$ is the singularity exponent and $f(q)$ the corresponding singularity dimension as defined in Eqs. (5) and (6).

which captures the uncertainty of the neural network’s weight parameters, θ , towards the end of the training process. This entails fitting an approximate Gaussian distribution to the observed changes of θ during the gradient descent process [135].

The neural network utilized in this study comprised three hidden layers with dimensions of 256, 128, and 128, employing the rectified linear unit (ReLU) [136] as the activation function. We arrived at this specific architecture after carefully observing the performance of various architectures during both the training and evaluation phases. The network generates membership scores for each of the five classes as a “logit vector,” denoted as $Z_i = f_\theta(X_i)$, with values subsequently related to model probabilities $p_{i,k}$ through a normalized exponential (softmax) function [137],

$$p_{i,k} = \frac{\exp(z_{i,k})}{\sum_k \exp(z_{i,k})}. \quad (10)$$

For machine learning, we created and extracted MFS features from the 10000 cascade series for each type. This dataset was subdivided into a training dataset comprising 9,800 samples per type and validation and test datasets comprising 100 samples per type each. To train the neural network, we conducted 800 epochs, systematically shuffling the training dataset and dividing it into batches of size 256, with each epoch representing one pass through the entire training dataset. The network weights are iteratively updated with each batch to minimize the loss function [Eq. (10)], employing the Adam optimizer with a learning rate decaying from 10^{-3} to 10^{-4} . In the final 100 epochs, we estimated SWAG [135], involving the determination of a Gaussian probability density function on the network weights θ . These parameters were chosen via optimization of the neural network performance on the validation dataset, while the results reported hereafter are obtained from the separate test set.

III. RESULTS

A. An admixture of additivity and multiplicative interactions produce diversity in cascade processes

Upon visually inspecting the apparent shape of resulting cascade processes, intriguing patterns emerged in the behavior of processes exclusively characterized by additive, multiplicative, and additomultiplicative interactions. Exclusive additivity notably tended to produce cascade time series with remarkable similarity (Fig. 4). Conversely, exclusively multiplicative interactions yielded highly non-Gaussian time series, displaying pronounced deviations from typical Gaussian distributions (Fig. 5). These cascade time series exhibited striking similarity, featuring tightly clustered fluctuations. However, the intricate interplay between additivity and multiplicative interactions emerged as a crucial factor in generating a diverse spectrum of cascade time series. Additomultiplicative cascades showcased a superior amalgamation of non-Gaussian characteristics and tightly clustered fluctuations. This intricate blend gave rise to a rich tapestry of data patterns closely resembling those observed in real-world contexts, highlighting the importance of considering such

interaction blends in modeling and comprehending adaptive biological and psychological phenomena (Fig. 6).

B. Multifractal spectral features loaded onto the principal components in varying ways depending on the cascade type

Our initial investigation explored the cross-correlation dynamics among the 13 multifractal spectral features for awGn cascades. Notably, these relationships exhibited an assortment of strengths, ranging from highly positive (depicted in shades of *blue*) to notably negative (depicted in shades of *brown*; Fig. 7). This diversity underscores the importance of incorporating multiple, rather than singular, multifractal spectral features in causal modeling. Furthermore, these associations were dynamic, exhibiting variations across additive (Fig. 7, *top left*), additomultiplicative (Fig. 7, *top right*), and multiplicative awGn cascades (Fig. 7, *top middle*)—in sequential order—each comprising the same underlying constituent noises. A key observation was the progressive weakening of these relationships from additive to multiplicative to additomultiplicative awGn cascades. This trend suggests that the correlation among multifractal spectral features diminishes as the interactions become more heterogeneous. Alternatively, one could interpret this decline in correlation coefficients as indicative of multifractal spectral features encoding more varied aspects of the multifractal structure in more heterogeneous cascades.

We then examined the loadings of the 13 features along the first two principal components, PC1 and PC2. As expected, the features exhibited distinct loadings across the additive (Fig. 7, *bottom left*), multiplicative (Fig. 7, *bottom middle*), and additomultiplicative (Fig. 7, *bottom right*) awGn cascades. For instance, the left-side height of the original spectrum, $\Delta f(\alpha)_{\text{Left}}$, width of the original spectrum, $\Delta\alpha$, and the horizontal location of the singularity, $\alpha_{f(\alpha)=1}$, showed the largest loadings on PC1, and $\Delta\alpha$, the height of the original spectrum, $\Delta f(\alpha)$, and $\Delta\alpha$ showed the largest loadings on PC2 for additive, multiplicative, and additomultiplicative awGn cascades, respectively (see Table II). Interestingly, even the most commonly used features $\Delta\alpha$ and multifractal nonlinearity, \mathcal{T}_{MF} , loaded differently across the three types of awGn cascades, although both these features always loaded heavily on PC1 for additive and multiplicative awGn cascades and on PC2 for additomultiplicative awGn cascades. While most features displayed positive loading either along PC1 or PC2, grouping features with similar factor loadings revealed variations across the additive, multiplicative, and additomultiplicative awGn cascades. Finally, the first four components were enough to explain more than 95% variance in the multifractal structure in each case: additive (Fig. 8, *left*), multiplicative (Fig. 8, *middle*), and additomultiplicative (Fig. 8, *right*). This implies that regardless of which features loaded onto the first two principal components, a highly correlated structure existed among these multifractal spectral features for each type of awGn cascade.

Figures 9–12 report the cross-correlation matrices and feature loadings for fGn, fractalizing, defractalizing, and mixed noise cascades. Similar patterns of results were observed for all four types of cascades. Key findings included variations in how different features loaded onto the first two principal components, with features exhibiting positive loadings also

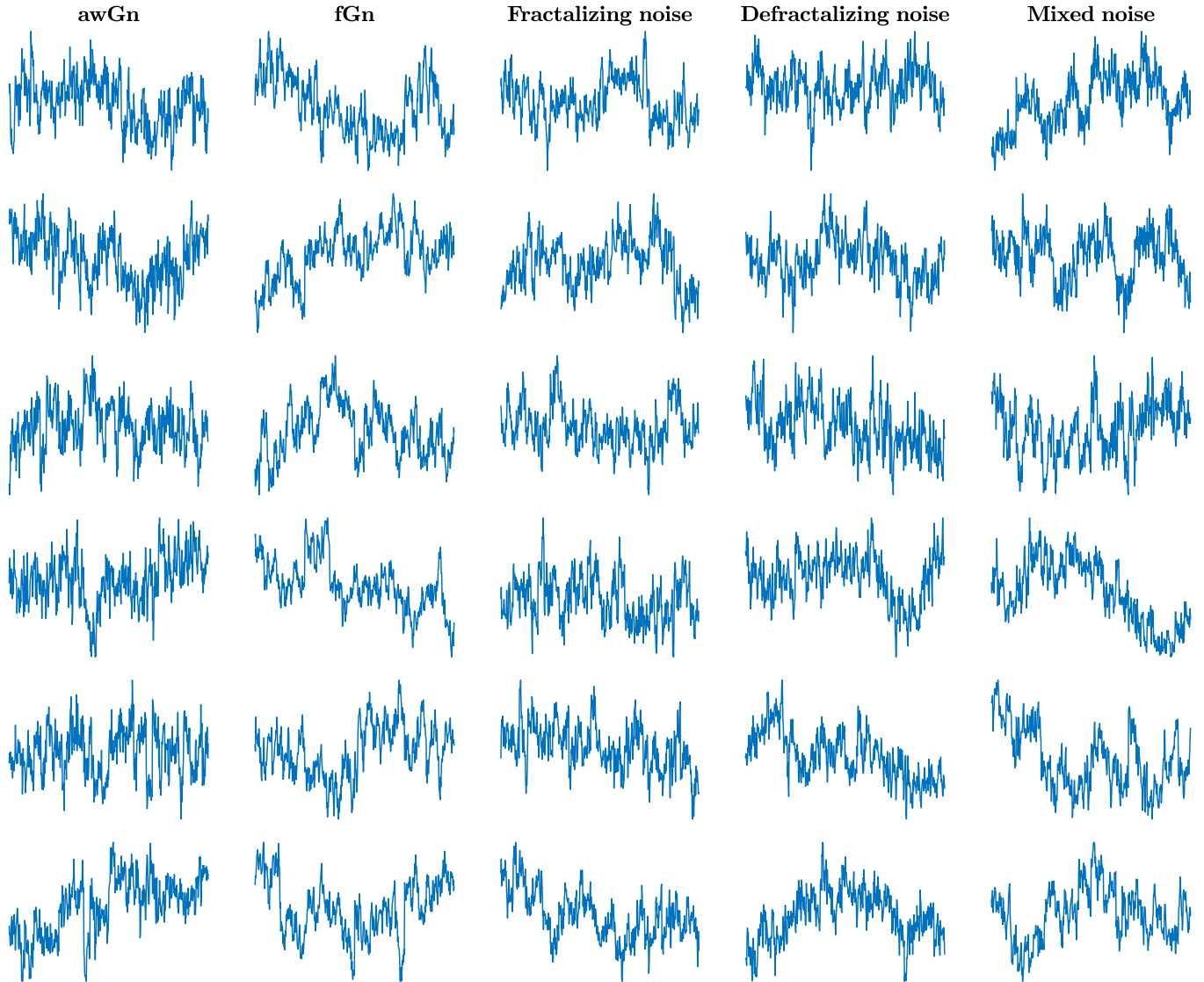


FIG. 4. Representative time series of the five types of random additive cascades in the tenth generation.

differing across the various constituent noise types. Nonetheless, these features showed an extreme diversity of their loading patterns based not just on the constituent noise but also on whether the interactions among these noises were additive, multiplicative, or additomultiplicative (*left, middle, and right* panels in Figs. 9–12). Overall, we observed significant variability in the rank order of the multifractal spectral features as they loaded onto PC1 and PC2 across the different types of cascades (see Table II). However, in all cases, the first four components were sufficient to explain more than 95% of the variance in the multifractal structure: additive (Fig. 8, *left*), multiplicative (Fig. 8, *middle*), and additomultiplicative (Fig. 8, *right*). These PCA results further support the notion that despite variations in feature loading onto the first two principal components, a highly correlated structure among multifractal spectral features exists for each cascade type. However, this correlated structure exhibits considerable variability depending on the type of noise and the interactions that contribute to the emergent multifractal structure.

C. Neural networks struggled to classify multiplicative cascade processes

We trained an “omnibus” neural network exclusively to predict the cascade model based on 13 distinct features extracted from the multifractal spectrum. In Fig. 13, we present the confusion matrix illustrating the likelihood of the network predicting each true class (columns) as one of the 15 classes (rows). Therefore, the probabilities for correct predictions can be retrieved from the diagonal entries. The confusion matrices reveal that the network demonstrates an overall rather low accuracy of 45.5% in accurately identifying the cascade model. Accuracy varied significantly across the 15 types of cascades: additive (fGn 49%, awGn 54%, fractalizing 45%, defractalizing 68%, mixed 61%), multiplicative (fGn 47%, awGn 20%, fractalizing 69%, defractalizing 46%, mixed 61%), and additomultiplicative cascades (fGn 55%, awGn 38%, fractalizing 40%, defractalizing 19%, mixed 10%). We observed a general drop in accuracy for the additomultiplicative case and poor

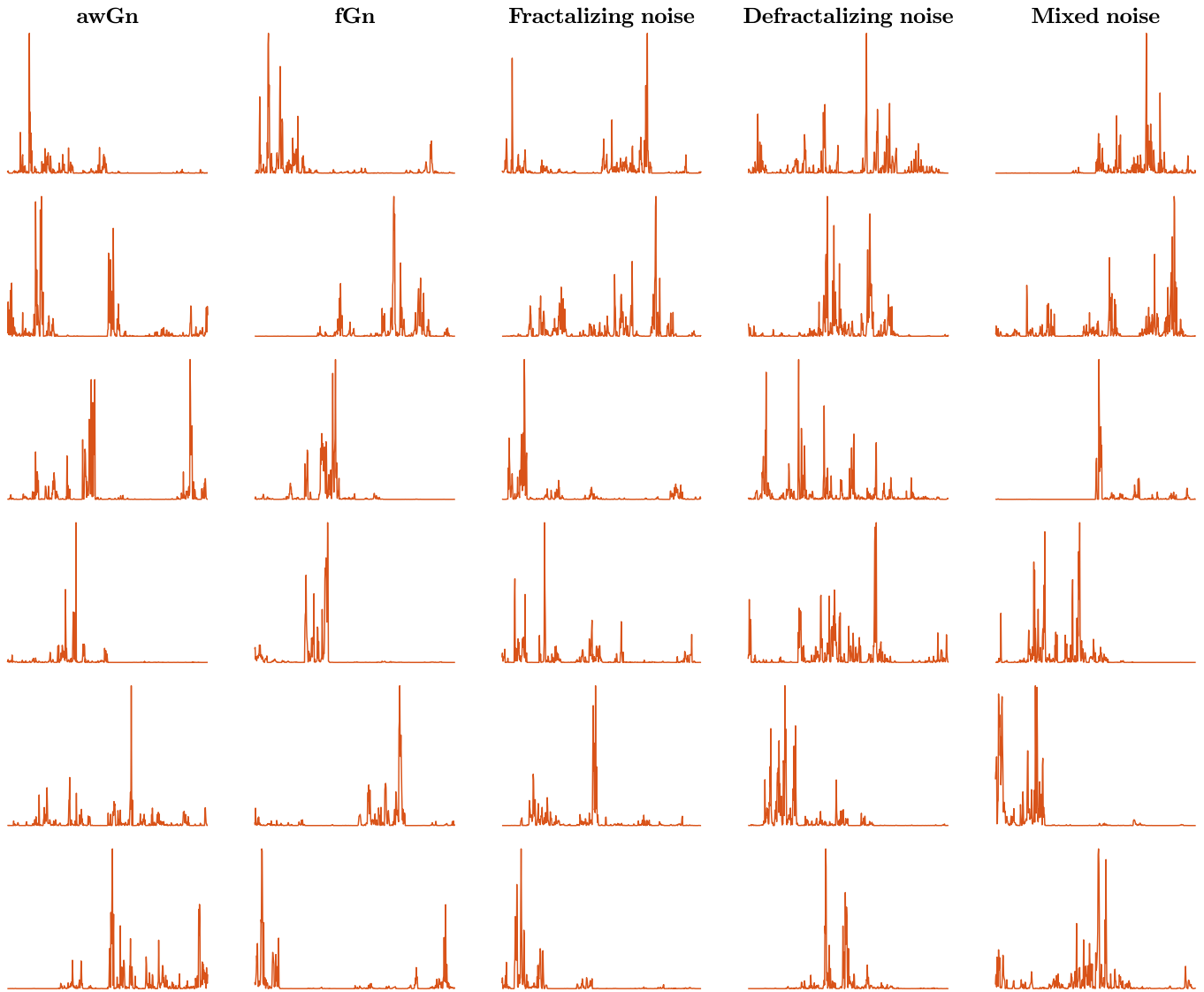


FIG. 5. Representative time series of the five types of random multiplicative cascades in the tenth generation.

accuracy for multiplicative fGn and additomultiplicative mixed noise cascades.

Next, we evaluated the performance of the same neural network, specifically for classifying additive, multiplicative, and additomultiplicative cascades, distinguishing them based on their constituent noises. When applied solely to additive cascades, the model achieved a remarkably high accuracy of 91.6% (Fig. 14, top left). However, this accuracy decreased to 75.4% for multiplicative cascades and 70.6% for additomultiplicative cascades. Interestingly, in each case, the accuracy was highest for the fractalizing scenario (0.98, 1.0, and 0.99, respectively) and lowest for the mixed case (0.85, 0.65, and 0.41, respectively). Training the network after removing only additive, multiplicative, or additomultiplicative cascades resulted in yet lower but consistent accuracy, hovering around 50% (specifically, 55.5%, 52.2%, or 55.0% after removing additive, multiplicative, or additomultiplicative cascades, respectively; Fig. 14, bottom). Therefore, it appears that multiplicative interactions override the actual properties of the constituent noise, making it difficult to discriminate among

the various cascade types in the multiplicative and additomultiplicative cases. Moreover, the admixture of additive and multiplicative cascades further accentuated this issue.

A significant advantage of feature-based machine learning, compared to non-feature-based approaches applied directly to raw sensor data utilizing convolutional or recurrent architectures [138], is its enhanced interpretability. Feature-based machine learning enables the identification of each feature’s impact on the neural network’s performance. For instance, one can selectively manipulate a feature, change its position among the inputs, and observe the resulting decrease in accuracy attributed to this feature’s misplacement. More broadly, one can rank the various features based on their importance to the model. Table III illustrates the feature importance for all seven neural networks, revealing several noteworthy trends. The most crucial feature was $\alpha_{f(\alpha)=1}$ for the overall network model, which remained consistent across all other six models except when considering only additive cascades. In that case, $\Delta\alpha_{\text{Left}}$ emerged as the most important feature, consistent with the previous finding that additive interactions

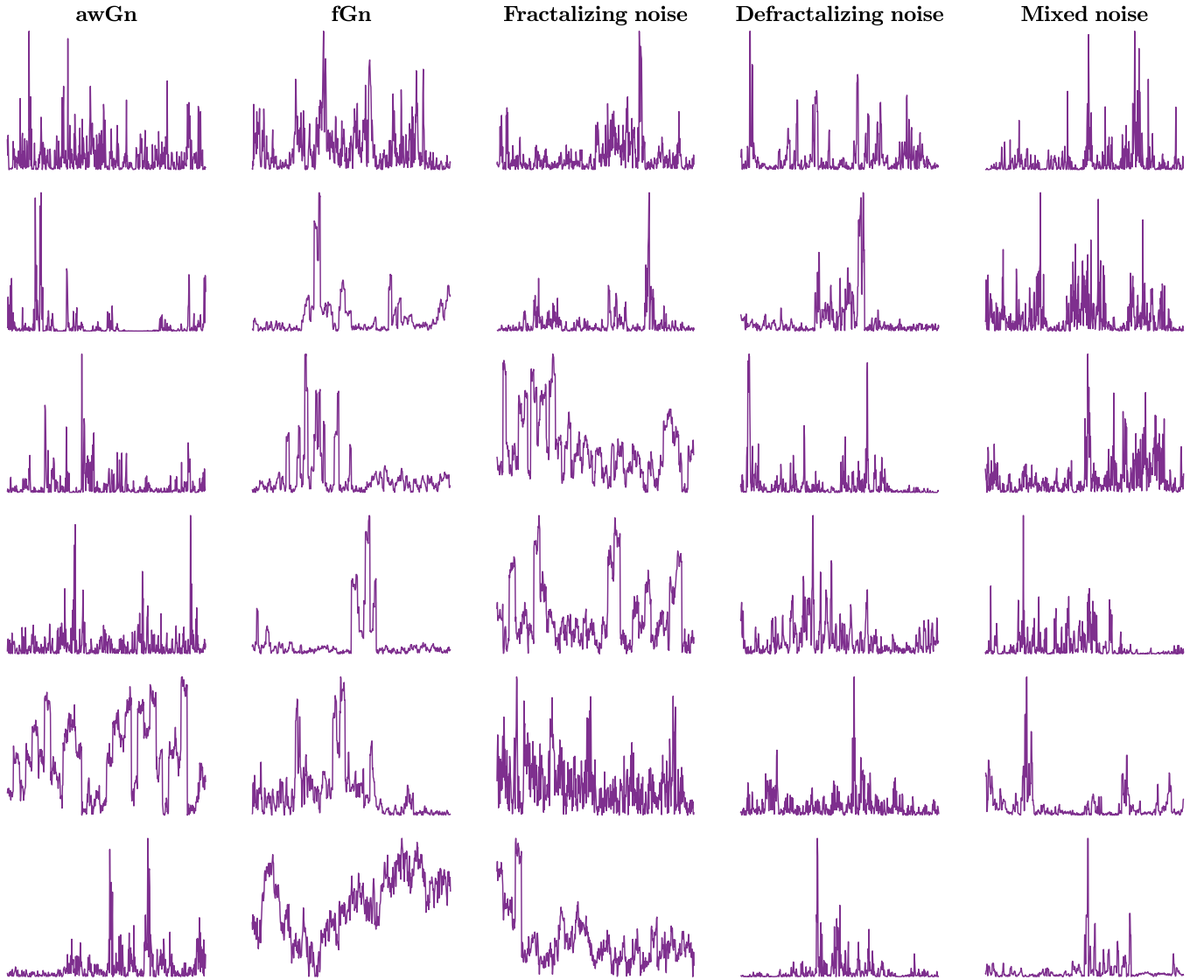


FIG. 6. Representative time series of the five types of random additumultiplicative cascades in the tenth generation.

TABLE III. Multifractal spectral feature importance for the seven neural networks classifying different cascade types.

All	Only			Without		
	Additive	Multiplicative	Additumult.	Additive	Multiplicative	Additumult.
$\alpha_{f(\alpha)=1}$	$\Delta\alpha_{\text{Left}}$	$\alpha_{f(\alpha)=1}$	$\alpha_{f(\alpha)=1}$	$\alpha_{f(\alpha)=1}$	$\alpha_{f(\alpha)=1}$	$\alpha_{f(\alpha)=1}$
$\Delta f(\alpha)_{\text{Left}}$	$\alpha_{f(\alpha)=1}$	$\Delta\alpha_{\text{Left}}$	$\Delta\alpha_{\text{Surr}}$	$\Delta\alpha_{\text{Left}}$	$\Delta\alpha_{\text{Left}}$	$\Delta\alpha_{\text{Surr}}$
$\Delta\alpha_{\text{Left}}$	$\Delta\alpha$	$\Delta\alpha_{\text{Surr}}$	$\Delta\alpha_{\text{Left}}$	$\Delta\alpha_{\text{Surr}}$	$\Delta f(\alpha)_{\text{Left}}$	N_{Spec}
N_{Spec}	$\Delta f(\alpha)_{\text{Left}}$	$\Delta f(\alpha)_{\text{Left}}$	$\Delta\alpha$	N_{Spec}	$\Delta\alpha$	$\Delta\alpha_{\text{Left}}$
$\Delta\alpha$	$\Delta f(\alpha)_{\text{Right}}$	$\Delta\alpha_{\text{Right}}$	$\Delta f(\alpha)_{\text{Left}}$	$\Delta f(\alpha)_{\text{Left}}$	$\Delta f(\alpha)_{\text{Right}}$	$\Delta f(\alpha)_{\text{Left}}$
$\Delta\alpha_{\text{Surr}}$	N_{Spec}	N_{Spec}	N_{Spec}	$\Delta\alpha_{\text{Right}}$	N_{Spec}	$\Delta\alpha_{\text{Right}}$
$\Delta f(\alpha)_{\text{Right}}$	$\Delta f(\alpha)$	$\Delta\alpha$	$\Delta\alpha_{\text{Right}}$	$\Delta\alpha$	$\Delta f(\alpha)$	$\Delta\alpha$
$\Delta\alpha_{\text{Right}}$	$\Delta\alpha_{\text{Surr}}$	$\Delta f(\alpha)_{\text{Right}}$	$\Delta f(\alpha)$	$\Delta f(\alpha)$	$\Delta\alpha_{\text{Surr}}$	$\Delta f(\alpha)_{\text{Right}}$
$\Delta f(\alpha)$	\mathcal{T}_{MF}	$\bar{\alpha}$	$\Delta f(\alpha)_{\text{Right}}$	$\Delta f(\alpha)_{\text{Right}}$	$\Delta\alpha_{\text{Right}}$	$\Delta f(\alpha)$
\mathcal{T}_{MF}	$\Delta\alpha_{\text{Right}}$	\mathcal{T}_{MF}	\mathcal{T}_{MF}	\mathcal{T}_{MF}	\mathcal{T}_{MF}	\mathcal{T}_{MF}
$\Delta f(\alpha)_{ \text{Left}-\text{Right} }$	$\Delta f(\alpha)_{ \text{Left}-\text{Right} }$	$\Delta f(\alpha)$	$\Delta f(\alpha)_{ \text{Left}-\text{Right} }$	$\overline{f(\alpha)}$	$\Delta f(\alpha)_{ \text{Left}-\text{Right} }$	$\overline{f(\alpha)}$
$\overline{f(\alpha)}$	$\overline{f(\alpha)}$	$\overline{f(\alpha)}$	$\overline{f(\alpha)}$	$\Delta f(\alpha)_{ \text{Left}-\text{Right} }$	$\overline{f(\alpha)}$	$\overline{f(\alpha)}$
$\bar{\alpha}$	$\bar{\alpha}$	$\Delta f(\alpha)_{ \text{Left}-\text{Right} }$	$\bar{\alpha}$	$\bar{\alpha}$	$\bar{\alpha}$	$\Delta f(\alpha)_{ \text{Left}-\text{Right} }$

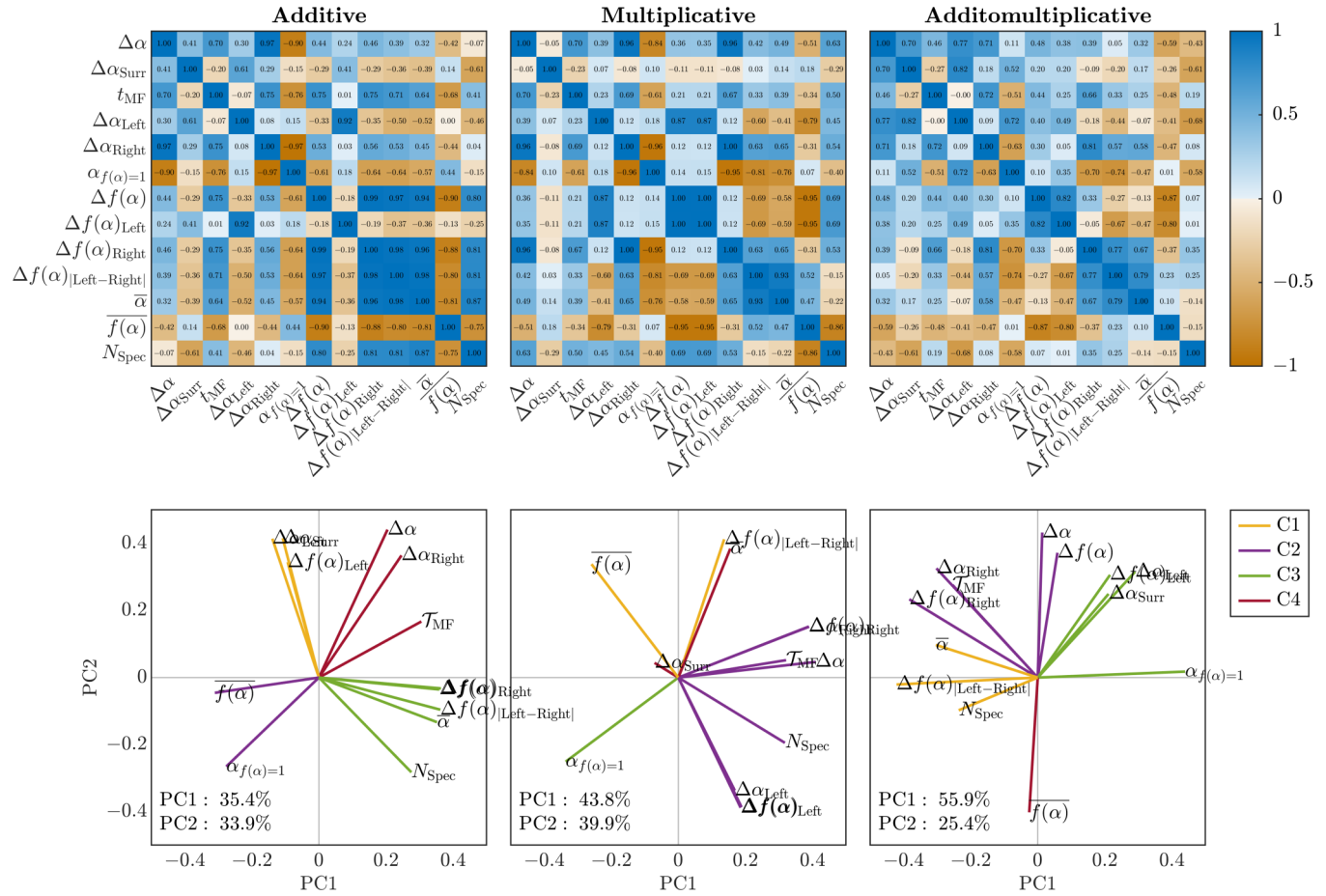


FIG. 7. Correlation matrices of multifractal spectral features for random additive (top left), multiplicative (top center), and additomultiplicative (top right) white noise cascades with additive white Gaussian noise, awGn, multipliers, and feature loading plots of the corresponding first two principal components (bottom). C1 through C4 represent the principal components grouped into four clusters using k -means clustering.

lead to leftward skewed spectra [44–46]. The multifractal spectral width, $\Delta\alpha$, and multifractal nonlinearity, T_{MF} , which are commonly utilized features for modeling the multifractal

structure of empirical measurements [126,139,140], did not feature among the top three features in either the “omnibus” model or the neural networks trained exclusively on additive,

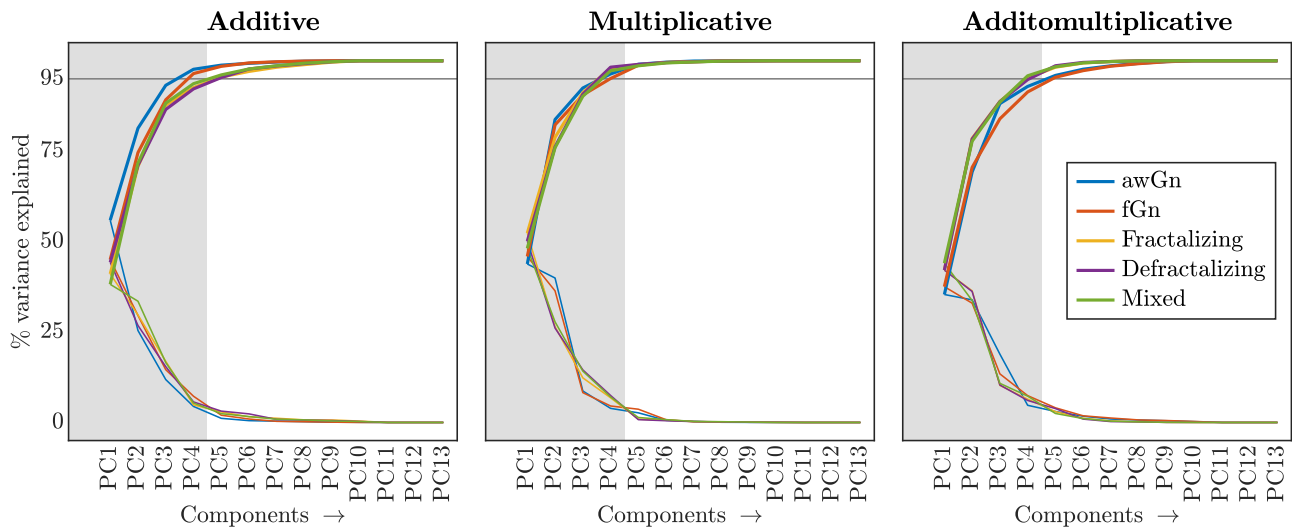


FIG. 8. Percentage variance explained by the 13 principal components for random additive (left), multiplicative (center), and additomultiplicative (right) cascades with the five types of constituent noises. the thick and thin lines denote the cumulative and individual variances.

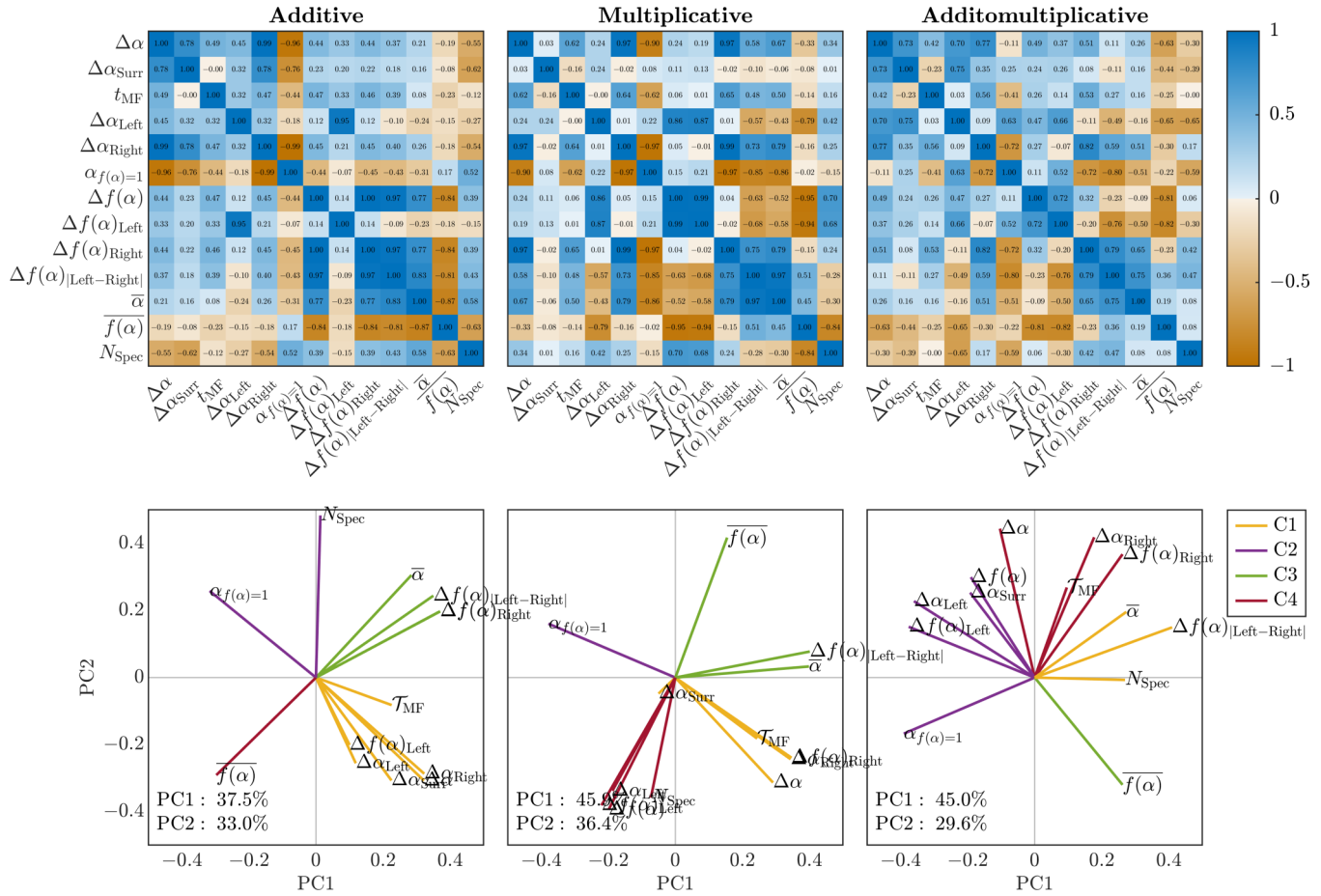


FIG. 9. Correlation matrices of multifractal spectral features for random additive (top left), multiplicative (top center), and additomultiplicative (top right) pink noise cascades with additive fractional Gaussian noise, fGn, multipliers, and feature loading plots of the corresponding first two principal components (bottom). C1 through C4 represent the principal components grouped into four clusters using *k*-means clustering.

multiplicative, and additomultiplicative cascades, even after excluding one of these types of cascades.

IV. DISCUSSION

Machine-learning models consistently demonstrate impeccable performance when trained on data from highly homogeneous and extreme populations, such as interbeat interval series comparing healthy adults to those diagnosed with chronic heart failure (e.g., [141–143]) or EEG signals comparing healthy adults to those diagnosed with schizophrenia (e.g., [144–146]). However, the efficacy of these models often plummets to chance levels when applied to more heterogeneous groups [20,21]. This study aimed to interrogate the notion that machine-learning models may inadequately encapsulate the intricacies inherent in physiological signals. It leverages the well-established understanding that physiological signals exhibit multifractal nonlinearity, stemming from multiplicative interactions across diverse spatial and temporal scales. Specifically, this investigation focuses on the multifractal properties as features intrinsic to 15 distinct types of binomial cascade processes generated by a spectrum of noise processes, including awGn, fGn, and various amalgamations. These processes exhibit additivity and multiplicative interactions, with a stochastic fusion of the two interaction types

occurring across constituent noise processes at diverse scales that we call additomultiplicative. Cross-correlation analysis applied to diverse multifractal spectral features reveals that these features adeptly capture nuanced aspects of the cascading time series, demonstrating minimal redundancy. Principal component analysis, employed across 13 distinct multifractal spectral features, reveals multiple routes to the emergent multifractal structure within these cascade processes. Fully connected neural networks unexpectedly struggled to classify the 15 distinct types of cascade processes based on the respective multifractal spectral features (45.5% accuracy) yet demonstrated improved accuracy when confronted only with additive (91.6%), multiplicative (75.4%), or additomultiplicative (70.6%) ones. These findings imply that, while traditional principal component analysis reveals distinct loadings attributed to individual noise processes, the multiplicative nature effectively conceals constituent processes from neural networks. This suggests that neural networks may lack the hierarchical depth required to effectively distinguish between diverse cascading processes, potentially limiting their utility in studying biological and physiological phenomena that can be better modeled as cascade dynamics.

The primary finding of note revolves around the cross-correlation analysis applied to a diverse array of multifractal spectral features, revealing their adeptness in capturing

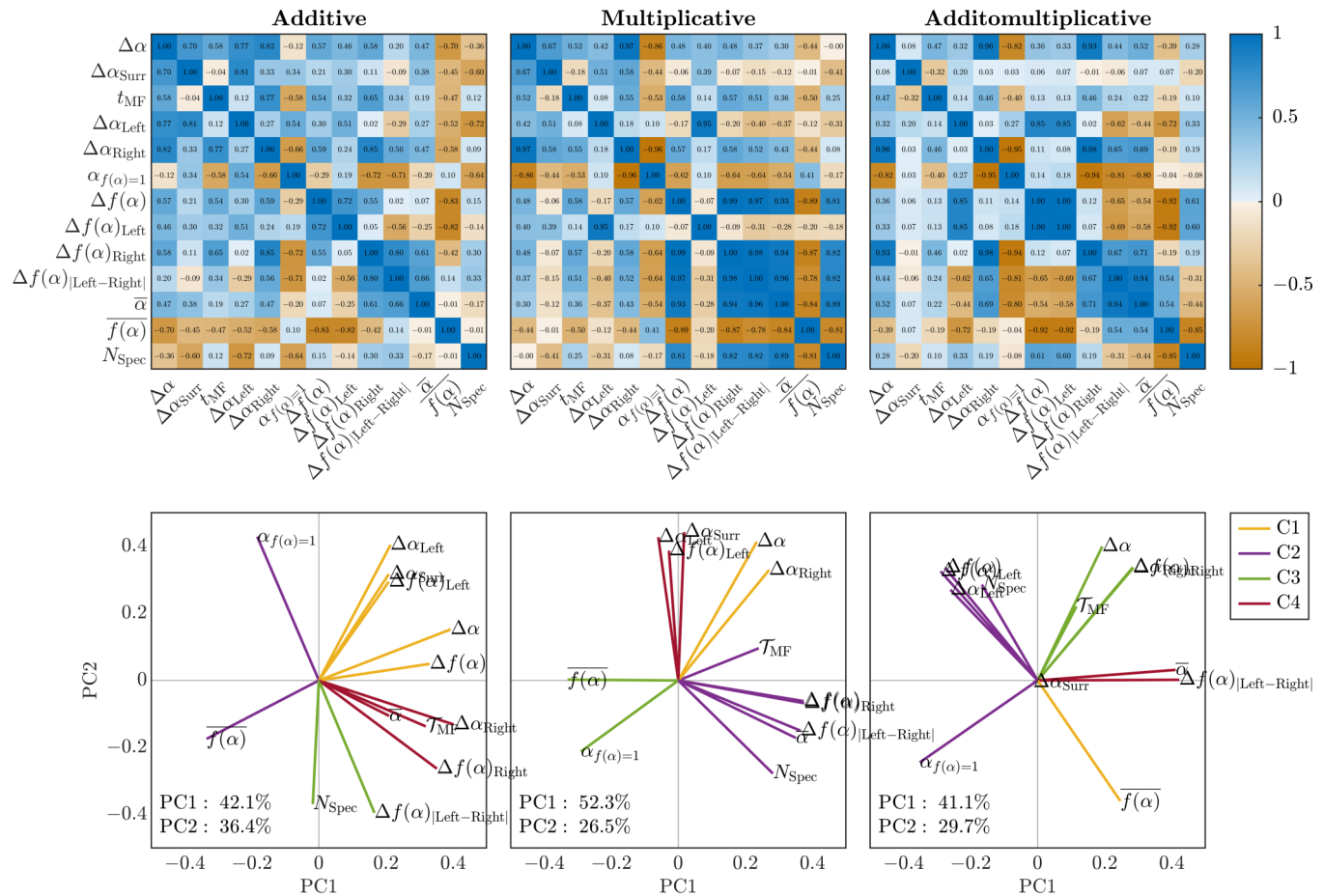


FIG. 10. Correlation matrices of multifractal spectral features for random additive (*top left*), multiplicative (*top center*), and additomorphic (*top right*) fractalizing noise cascades with anticorrelated Gaussian noise multipliers characterized by fGn, $H_{\text{fGn}} = 0$, and incrementally increasing H_{fGn} to 1 across 15 generations, and feature loading plots of the corresponding first two principal components (*bottom*). C1 through C4 represent the principal components grouped into four clusters using k -means clustering.

nanced aspects of cascading time series with minimal redundancy. Traditionally, multifractal spectrum analysis has predominantly focused on two facets: the width of the multifractal spectrum and the disparity between the spectrum widths of the original time series and those of its surrogates, computed as either $\Delta_{\text{Orig}} - \Delta_{\text{Surr}}$ [126] or as \mathcal{T}_{MF} [48,139]. Additionally, some researchers have advocated considering asymmetry in the multifractal spectrum to interpret distortions in the hierarchical organization of complex multiplicative processes (e.g., [147,148]). While these conventional multifractal spectral features may offer valuable insights and potentially represent the most salient characteristics of multifractal structure, the relatively weak and uniform correlation relationships observed among the 13 multifractal spectral features incorporated in the present study suggest that these features might not fully capture the diversity within multifractal structure. Therefore, there could be analytical merit in incorporating these additional features. However, elucidating interpretive explanations regarding the specific determinants of each feature remains elusive, precluding theoretically informed use of these features beyond brute-force machine-learning applications. Future endeavors could enhance our comprehension of the significance of each multifractal spectral feature in terms

of time series heterogeneity, thus facilitating their utilization in modeling stochastic cause and effect.

The second noteworthy finding pertains to the distinctive loading patterns observed across various multifractal spectral features along the first two principal components. These loading patterns exhibited clear distinctions among cascades comprising different types of noise interactions across generations, reflecting processes occurring at diverse spatial and temporal scales, including awGn, fGn, fractalizing, defractalizing, and mixed noises. Moreover, these loading patterns effectively differentiated between additive, multiplicative, and additomorphic interactions across these diverse noise processes. Thus, the diverse multifractal spectral features conveyed distinct information types, reflecting heterogeneity's unique aspects across different cascades. We had previously noted that, while traditional features, often employed in linear causal modeling [149–151], tend to disrupt ergodicity, multifractal descriptors, in contrast, exhibit ergodicity [47–51], thereby offering a dependable and consistent set of causal predictors of the adaptive biological and psychological function [60,63–67,69–71,152–154]. The current discovery that multifractal spectral features can delineate distinct patterns of heterogeneity, capturing both the constituent noise and

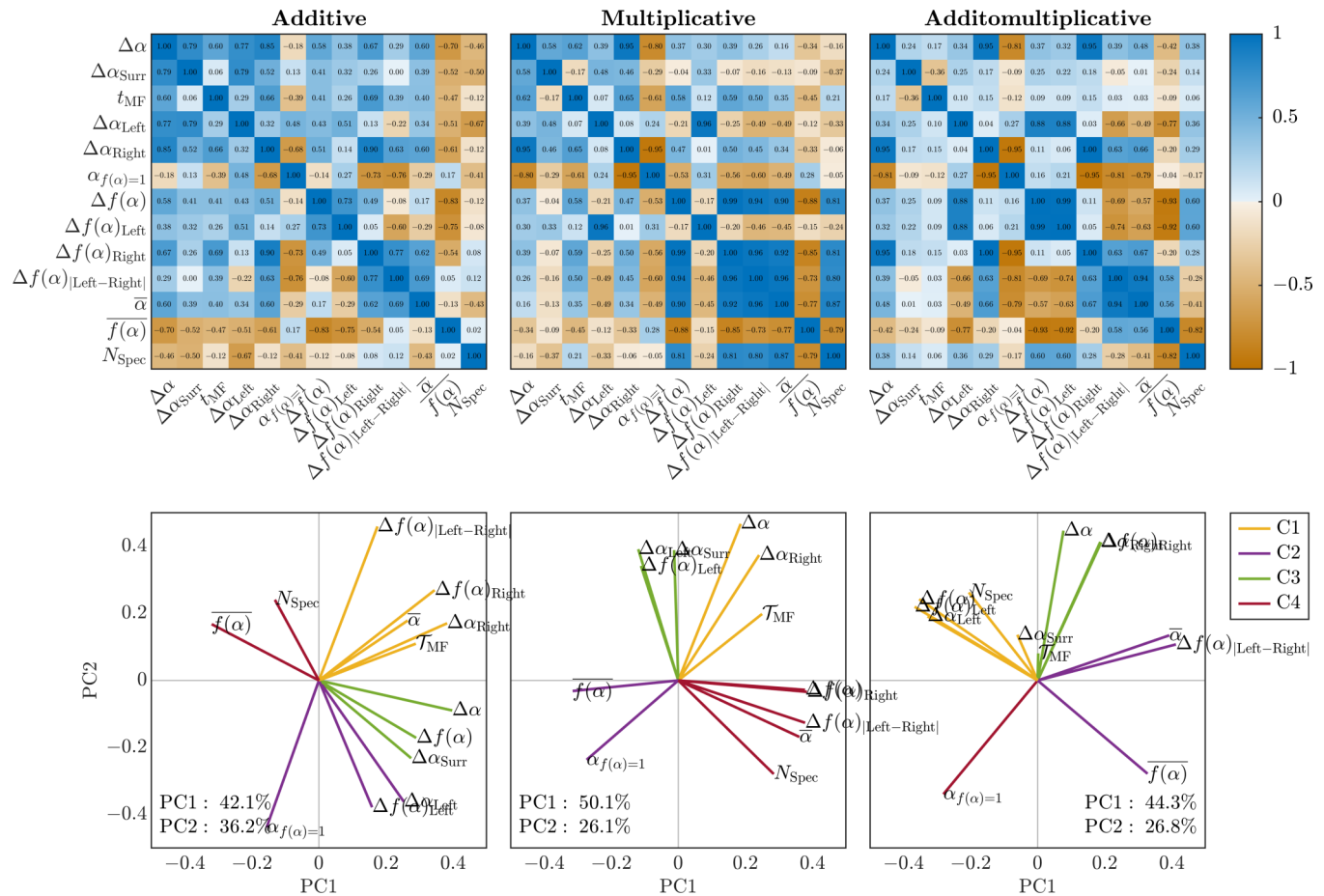


FIG. 11. Correlation matrices of multifractal spectral features for random additive (top left), multiplicative (top center), and additumultiplicative (top right) defractalizing noise cascades with correlated Gaussian noise multipliers characterized by fGn, $H_{\text{fGn}} = 1$, and gradually decreasing H_{fGn} to 0 across 15 generations, and feature loading plots of the corresponding first two principal components (bottom). C1 through C4 represent the principal components grouped into four clusters using k -means clustering.

the nature of interactions—whether additive, multiplicative, or various amalgamations—lends credence to these modeling endeavors. It implies that incorporating multifractal descriptors as causal factors in modeling adaptive biological and psychological functions can unveil mechanisms that may remain obscured by summarizing stochastic time series using alternative descriptors [155].

The third and final notable finding pertains to the performance of neural networks in discriminating among the 15 cascade types. Surprisingly, these neural networks encountered difficulties classifying the distinct types of cascade processes, achieving only 45.5% accuracy when confronted with additive, multiplicative, and additumultiplicative cascades simultaneously. Nonetheless, the accuracy of these neural networks significantly improved when confronted solely with classifying cascades of different noise types within the additive category (91.6%), the multiplicative category (75.4%), or the additumultiplicative (70.6%) category of cascades. These difficulties resembled previous performance of fully connected neural networks in discerning between five prominent models of anomalous diffusion trajectories [52]. Anomalous diffusion trajectories deviate from Fick’s theory

of diffusion, exhibiting a power-law pattern of mean squared displacement ($\langle x^2(t) \rangle \propto t^\alpha$ with $\alpha \neq 1$), and this previous study included five diffusion models: fractional Brownian motion (FBM), scaled Brownian motion (SBM), controlled-time random walk (CTRW), annealed transient time motion (ATTM), and Lévy walk (LW) [9,156]. We had previously also reported the widespread presence of multifractal structures within these diffusion models, suggesting a common origin within a cascade-dynamical framework [51]. Therefore, the ability of neural networks to differentiate between these models based on multifractal characteristics aligned well with prior expectations and findings in the field. The present performance of neural networks proved disappointing, indicating that these cascades might be more intricate and hierarchical than diffusion models. Indeed, the failure of neural networks to differentiate between various cascade models may be attributed to the multiplicative nature of these cascades, which may effectively conceal the constituent processes from the neural networks. This suggests that neural networks may lack the hierarchical depth necessary to effectively distinguish between diverse cascading processes, potentially limiting their applicability in studying biological and physiological

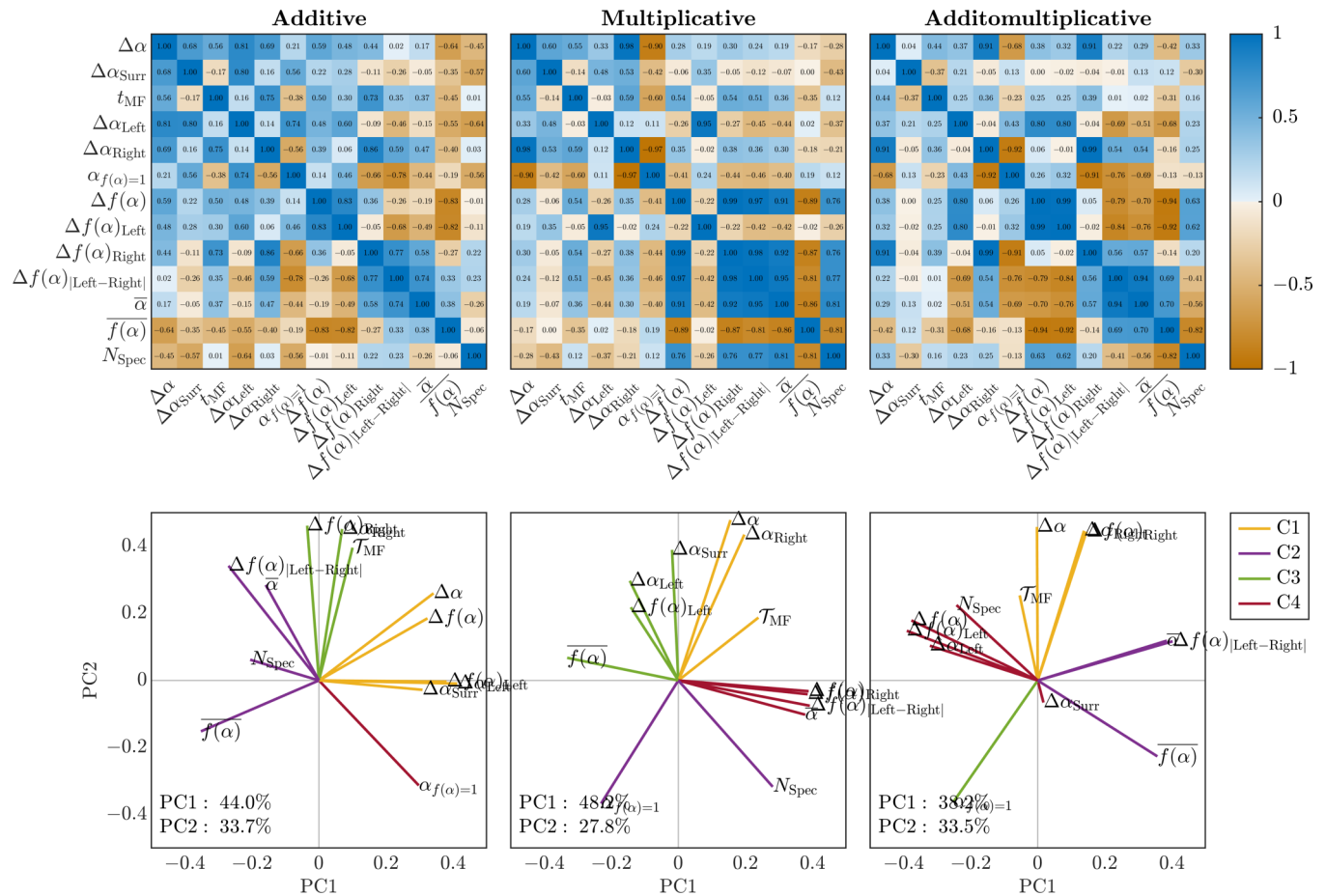


FIG. 12. Correlation matrices of multifractal spectral features for random additive (top left), multiplicative (top center), and additumultiplicative (top right) mixed noise cascades with Gaussian noise multipliers characterized by either ideal fGn (i.e., $H_{\text{fGn}} = 0.5$) or ideal awGn (i.e., $H_{\text{fGn}} = 1$) randomly selected at each generation, and feature loading plots of the corresponding first two principal components (bottom). C1 through C4 represent the principal components grouped into four clusters using k -means clustering.

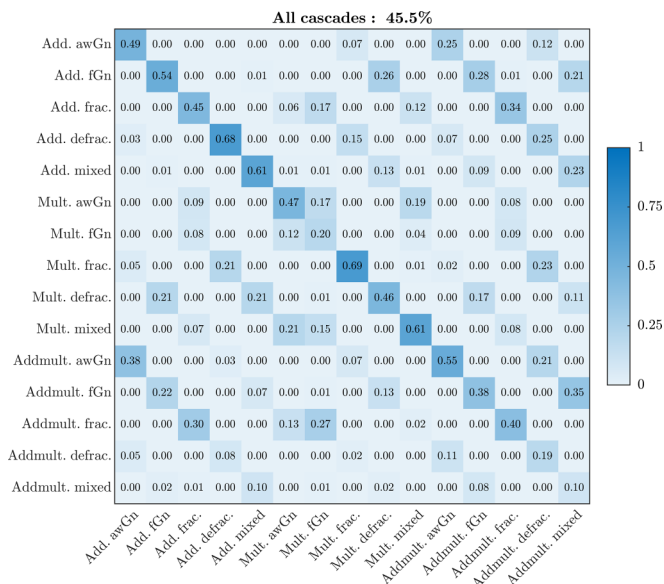


FIG. 13. Confusion matrix showing the accuracy of cascade classification across all cascade types. The values in each cell encode the likelihood of the network predicting each true class (columns) as one of the 15 classes (rows).

phenomena better represented by cascade dynamics. It may be useful in this case to supplement the multifractal features with more traditional features.

Instead, cascades that incorporate multifractal noise open up a field of theoretical inquiry that paves a path towards scaling a multifractal model of biological and psychological processes up from single observables to an entire organism; a path that network science has already begun to hint at [157]. The present exploration of cascades with multifractal noise is an early step in learning how to interpret our single observables' multifractality better. The present work does not give indicators of network topology; instead, it offers a view of how classic categories of cascades (i.e., additive and multiplicative) react to and involve multifractal noise that might spread through the system from spatiotemporally neighboring points of cascade dynamics. This work informs this line of theoretical inquiry by indicating that the mathematical form of cascade dynamics (i.e., additive or multiplicative) radically changes the effect of the simulated observable absorbing multifractal noise. For instance, we confirmed a previous finding that multiplicative cascades show stronger \mathcal{T}_{MF} signatures of nonlinearity with progressively more generations [45,46]. However, multifractal cascades generate much stronger \mathcal{T}_{MF} signatures of nonlinearity with multifractal noise than less

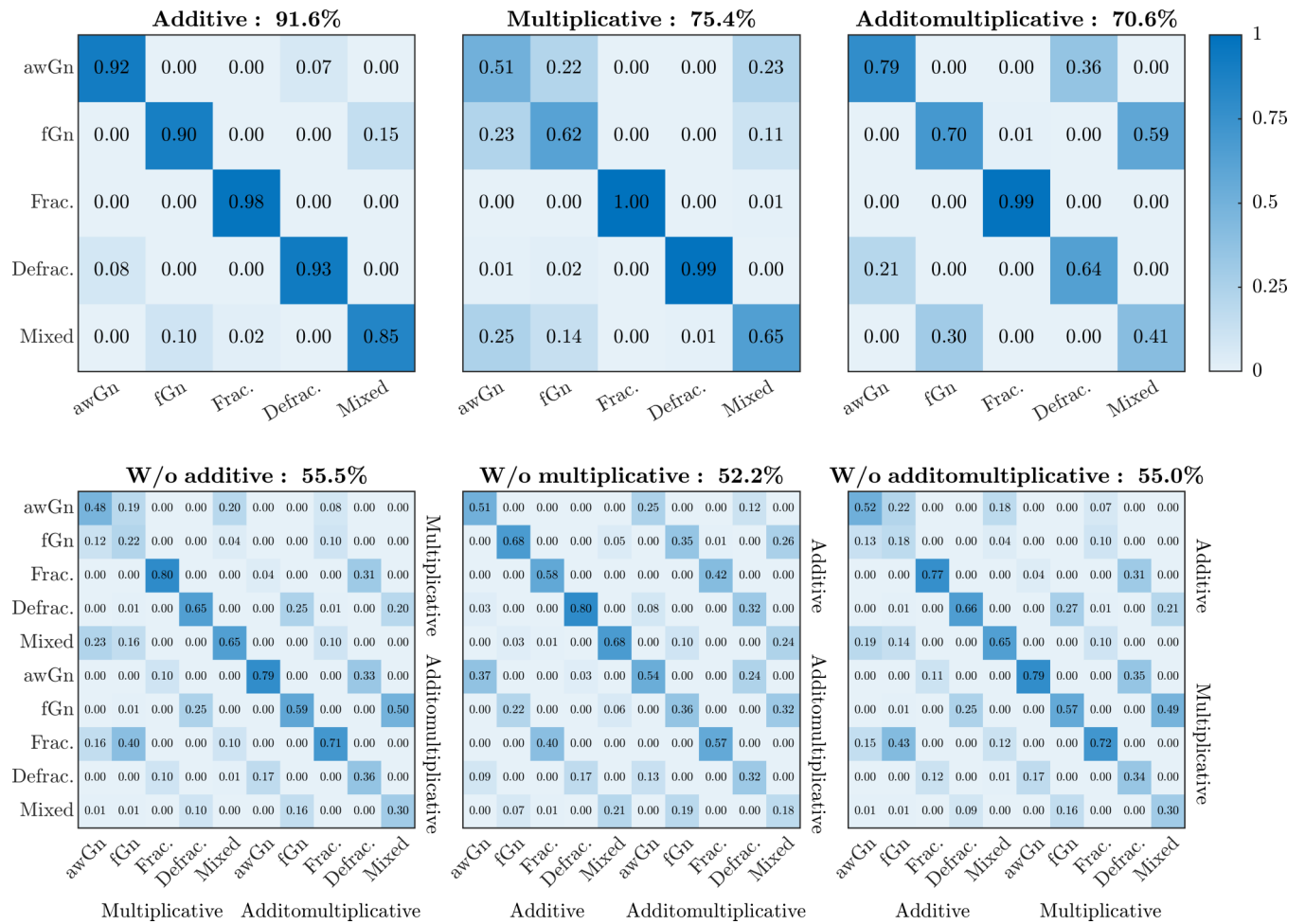


FIG. 14. Confusion matrices showing the accuracy of cascade classification within only the random additive (top left), multiplicative (top center), and additomultiplicative (top right) cascades and across all cascade types without using the random additive (bottom left), multiplicative (bottom center), and additomultiplicative (bottom right) cascades. The values in each cell encode the likelihood of the network predicting each true class (columns) as one of the 5 classes (rows).

multifractal IAAFT noise. This point extends the previous finding that multiplicative cascades involving fGn showed greater \mathcal{T}_{MF} than multiplicative cascades with awGn [46]. Hence, we may be able to rank order the strength of multifractal nonlinearity from the greatest to the least for multiplicative cascades involving multifractal noise with wider spectra or more nonlinear temporal correlations, multifractal noise with narrower spectra more closely approximating monofractal fGn, as well as awGn. This work also informs this approach by indicating that noise with greater multifractal spectrum width (e.g., in the comparison between nonlinearly multifractal noise and IAAFT noise) and greater nonlinear temporal correlations (i.e., in the contrast between nonlinearly multifractal noise and IAAFT noise) can promote specifically different forms of ergodicity breaking.

We must perceive organisms not as uniform entities but rather as intricate and task-responsive assemblages of numerous degrees of freedom [158,159]. Here, “degrees of freedom” denotes the myriad intricacies within a system that can vary and become accessible for control or adaptation in response to specific task constraints [160–163], thus illustrating cascading dynamics [164] that lead to the emergence of new adaptive

behaviors shaping the entire system [165–172]. Accordingly, network science has embarked on modeling multifractality as a refined representation of the cascade relationships that potentially govern an organism’s allocation of degrees of freedom; a notion supported both theoretically [157] and empirically [53–71]. Moreover, multifractality may encapsulate broader system properties beyond what a single observable can capture. The hierarchical structure implicit in any observable likely extends beyond that observable and reflects the aggregates influencing that observable. Therefore, there is reason to believe that the multifractal structure of any single observable should reflect not only the broader system containing it but also the novel interactions it engages in. Indeed, in our study involving the full-body motion of human participants during a perceptual task [70,153], basic network analyses revealed extensive connections among anatomical components, showcasing numerous pairwise relationships between current multifractality in one observable and subsequent multifractality in another. This empirical evidence suggests that multifractality in any observable may bear the signature of multifractality elsewhere in the system. The present “failure” of neural networks in discriminating

among the 15 cascade types implies that machine learning might presently lack the capability to facilitate investigations centered on the genesis of emergent multifractal structures in empirical biological and psychological measurements.

Hence, the current simulation is a pivotal stride in delineating the constraints of machine-learning models. We have illuminated the potential prematurity in employing machine learning for interpreting multifractal outcomes, particularly when expecting our cascade-like measurements to mirror multifractal signatures stemming from cascade processes occurring elsewhere within the same organism. While our simulation encompassed basic additive, multiplicative, and additomultiplicative cascades, refining the cascade structures to simulate diverse network interactions contributing to cascade dynamics could introduce further complexities as we strive to elucidate the nexus between distributed coordination and multifractal cascades [157]. This challenge is exacerbated by “stochastic resonance” or “noise-based” stimulation beyond conventional “white-noise” structures like awGn to encompass more inherently naturalistic fractal and multifractal forms of stimulation [74–77,173,174], which generate an enormous diversity of multifractal processes [44–46]. The theoretical advancements requisite to bring these insights into machine learning necessitate the development of capabilities to decipher the hierarchical characteristics of these cascade models [175].

Machine learning for networked flows of multifractality

A prominent challenge in applying machine-learning models to multifractal structures stems from the absence of well-defined expectations. On the one hand, insights gleaned from examining the multifractality of a single observable have potentially transcended simple discriminatory capacities, such as associating varying degrees of multifractality with health conditions (e.g., [87,176,177]). Indeed, machine learning has often successfully discriminated between health and disease states [90,102,103,178,179]. Nonetheless, nonlinear properties of a single observable may encapsulate aspects of an entire organism’s functioning, as seen in cases like Parkinson’s disease [72,73,180–183]. While one observable may seemingly exist independently, it could also function as part of a loosely interactive ensemble, where loose interactions among observables within the ensemble are permissible. For instance, simulation studies investigating individual cascade processes have been pivotal in elucidating the sequential variations observed when a person presses a button with their forefinger to signal one-second intervals [184,185]. This approach is fundamental in advancing a cascade-dynamical representation of finger behavior in such tasks. However, it is crucial to recognize that the pressing of a fingertip represents merely the immediate point of contact between the entire organism and the task environment. Acknowledging that a single button press is merely the surface manifestation of an organism-wide phenomenon, we understand that fingertip actions emerge from a vast network of anticipatory postural adaptations and longer-range postures distributed across the entire movement system [165–172]. Presumably, what we observe in a single observable reflects the endogenous flow of coordinating cascades from interconnected observables

within the organism alongside any exogenous stimulation (e.g., [74–77,173,174]). The spatiotemporal dissemination challenges our machine-learning endeavors, as they do not appear capable of diagnosing organism-wide flows from multifractal results derived from individual observables.

Two immediate avenues that have leveraged machine learning within the broader umbrella of multiscale modeling include understanding fundamental physics [15] and fine tuning parameters for established physics-based quandaries. Recent advancements showcase this potential: from employing data-driven approaches to resolve unexplained issues related to elasticity [11] to uncovering partial differential equations for various nonlinear dynamical systems [10,12–14]. While this domain holds significant promise, particularly when paired with deep learning, it necessitates a profound comprehension and direct engagement with the underlying learning machines [186]. The success of these attempts is partially due to the modeled systems following the so-called “low-dimensional chaos” wherein a few parameters can summarize the system’s entire dynamics. However, our observations’ underlying systems can exhibit a broader spatiotemporal structure [187,188]. Moreover, the fractal nature of these systems supports the theoretical notion that we should be able to extract global dynamics from the lower-dimensional projections manifested in our observations [189]. We have probably not exclusively selected observables with multifractal characteristics; rather, multifractal structure likely represents a more ubiquitous trait of the entire organismic system. The hierarchical arrangement implicit in any given observable is unlikely to be solely attributed to that specific observable; instead, it likely mirrors the collective interactions of numerous components, as demonstrated through our cascading numerical simulations. Whether the data-driven, physics-based machine-learning models can outperform the neural networks employed in the current study in classifying multifractal cascades remains to be determined.

Machine-learning techniques have exhibited remarkable prowess in image recognition, finding direct utility in diagnostics across electrophysiology, radiology, and pathology, leveraging extensively annotated datasets [190–194]. However, the efficacy of machine learning often wanes when tasked with prognosis, particularly in deciphering complex physiological time series. In this realm, classical physics-based simulation maintains its indispensable role. In taking stock of the foregoing analyses and tests, we have a few choices about where to seek the limitations and the routes for future investigation. On the one hand, we see a ceiling on the efficacy of multifractal features as classifiers, and this ceiling could signify a fundamental limit to what multifractal description can show. However, multifractality is the distinguishing feature of cascade dynamics, and multifractal geometry is the only known formalism for addressing cascade structures. So, either we need to look for elaborations of multifractal geometry (e.g., beyond the $f(\alpha)$ spectrum [195,196]), or we need to acknowledge potential limitations of machine learning [20,21]. On the latter point, we must concede that these architectures’ correlation metrics to support classification may not necessarily be the only ones or those best poised to classify cascade-driven ergodicity-breaking time series. On the other hand, principal component analysis showed finer sensitivity to

the different features contributing to multifractal nonlinearity, suggesting that, once we arrive at the ergodic description of cascade dynamics using multifractal geometry [47–51], these multifractal descriptors reveal how different categories of cascade exhibit different routes towards multifractal nonlinearity. Cascade dynamics exhibit systematicity at the level of ergodic descriptors via multifractal geometry, underscoring the need for future research to investigate the ergodicity of traditional classifiers and the performance of machine-learning architectures beyond correlation metrics [47–51]. In this study, we avoided using raw data for classification due to the ergodicity-breaking aspect of cascade dynamics, where short samples fail to capture long-term dynamics. Future work will explore whether applying deep learning and convolutional neural networks is better suited for modeling the hierarchical structure of cascade time series and addressing ergodicity-breaking phenomena. We aim to refine the machine-learning classification of raw ergodicity-breaking cascade time series, aligning them more accurately with this ergodic description and paving the way for more robust and insightful analyses.

No data were used for the research described in the article.

ACKNOWLEDGMENTS

M.M. was supported by the Center for Research in Human Movement Variability at the University of Nebraska at Omaha, funded by the National Institute of General Medical Sciences (NIGMS; Grant No. P20GM109090). H.S. was supported by the German Research Foundation (DFG; Grant No. 491466077).

Author contributions are as follows: M.M.: conceptualization, methodology, formal analysis, original draft, review & editing, visualization, project administration; H.S.: Formal analysis, review & editing; D.G.K.-S.: Conceptualization, methodology, original draft, review & editing.

The authors declare that they have no known competing financial interests or personal relationships that could have appeared to influence the work reported in this paper.

-
- [1] A. Esteva, A. Robicquet, B. Ramsundar, V. Kuleshov, M. DePristo, K. Chou, C. Cui, G. Corrado, S. Thrun, and J. Dean, A guide to deep learning in healthcare, *Nat. Med.* **25**, 24 (2019).
- [2] J. B. Heaton, N. G. Polson, and J. H. Witte, Deep learning for finance: Deep portfolios, *Appl. Stoch. Models Bus. Ind.* **33**, 3 (2017).
- [3] M. I. Jordan and T. M. Mitchell, Machine learning: Trends, perspectives, and prospects, *Science* **349**, 255 (2015).
- [4] A. Rajkomar, J. Dean, and I. Kohane, Machine learning in medicine, *N. Engl. J. Med.* **380**, 1347 (2019).
- [5] T. Wuest, D. Weimer, C. Irgens, and K.-D. Thoben, Machine learning in manufacturing: Advantages, challenges, and applications, *Prod. Manuf. Res.* **4**, 23 (2016).
- [6] C. Angermueller, T. Pärnamaa, L. Parts, and O. Stegle, Deep learning for computational biology, *Mol. Syst. Biol.* **12**, 878 (2016).
- [7] B. Alipanahi, A. DeLong, M. T. Weirauch, and B. J. Frey, Predicting the sequence specificities of DNA-and RNA-binding proteins by deep learning, *Nat. Biotechnol.* **33**, 831 (2015).
- [8] J. G. Greener, S. M. Kandathil, L. Moffat, and D. T. Jones, A guide to machine learning for biologists, *Nat. Rev. Mol. Cell Biol.* **23**, 40 (2022).
- [9] G. Muñoz-Gil, G. Volpe, M. A. Garcia-March, E. Aghion, A. Argun, C. B. Hong, T. Bland, S. Bo, J. A. Conejero, N. Firbas *et al.*, Objective comparison of methods to decode anomalous diffusion, *Nat. Commun.* **12**, 6253 (2021).
- [10] S. L. Brunton, J. L. Proctor, and J. N. Kutz, Discovering governing equations from data by sparse identification of nonlinear dynamical systems, *Proc. Natl. Acad. Sci. USA* **113**, 3932 (2016).
- [11] S. Conti, S. Müller, and M. Ortiz, Data-driven problems in elasticity, *Arch. Ration. Mech. Anal.* **229**, 79 (2018).
- [12] G. E. Karniadakis, I. G. Kevrekidis, L. Lu, P. Perdikaris, S. Wang, and L. Yang, Physics-informed machine learning, *Nat. Rev. Phys.* **3**, 422 (2021).
- [13] M. Raissi, P. Perdikaris, and G. E. Karniadakis, Machine learning of linear differential equations using Gaussian processes, *J. Comput. Phys.* **348**, 683 (2017).
- [14] M. Raissi and G. E. Karniadakis, Hidden physics models: Machine learning of nonlinear partial differential equations, *J. Comput. Phys.* **357**, 125 (2018).
- [15] S. H. Rudy, S. L. Brunton, J. L. Proctor, and J. N. Kutz, Data-driven discovery of partial differential equations, *Sci. Adv.* **3**, e1602614 (2017).
- [16] L. Messeri and M. Crockett, Artificial intelligence and illusions of understanding in scientific research, *Nature (London)* **627**, 49 (2024).
- [17] R. Aggarwal, V. Sounderajah, G. Martin, D. S. Ting, A. Karthikesalingam, D. King, H. Ashrafian, and A. Darzi, Diagnostic accuracy of deep learning in medical imaging: A systematic review and meta-analysis, *npj Digit. Med.* **4**, 65 (2021).
- [18] A. Madani, R. Arnaout, M. Mofrad, and R. Arnaout, Fast and accurate view classification of echocardiograms using deep learning, *npj Digit. Med.* **1**, 6 (2018).
- [19] I. S. Stafford, M. Kellermann, E. Mossotto, R. M. Beattie, B. D. MacArthur, and S. Ennis, A systematic review of the applications of artificial intelligence and machine learning in autoimmune diseases, *npj Digit. Med.* **3**, 30 (2020).
- [20] M. M. Bejani and M. Ghatee, A systematic review on overfitting control in shallow and deep neural networks, *Artif. Intell. Rev.* **54**, 6391 (2021).
- [21] A. M. Chekroud, M. Hawrilenko, H. Loho, J. Bondar, R. Gueorguieva, A. Hasan, J. Kambeitz, P. R. Corlett, N. Koutsouleris, H. M. Krumholz *et al.*, Illusory generalizability of clinical prediction models, *Science* **383**, 164 (2024).
- [22] F. Doshi-Velez and B. Kim, Towards a rigorous science of interpretable machine learning, [arXiv:1702.08608](https://arxiv.org/abs/1702.08608).
- [23] Z. C. Lipton and J. Steinhardt, Troubling trends in machine learning scholarship: Some ML papers suffer from flaws that

- could mislead the public and stymie future research, *Queue* **17**, 45 (2019).
- [24] C. P. Rosé, E. A. McLaughlin, R. Liu, and K. R. Koedinger, Explanatory learner models: Why machine learning (alone) is not the answer, *Br. J. Educ. Technol.* **50**, 2943 (2019).
- [25] E. Jablonka, Interacting networks in social landscapes: A devo-evo approach to socialcultural dynamics, *Hum. Dev.* **67**, 288 (2023).
- [26] D. J. Nicholson and J. Dupré, *Everything Flows: Towards a Processual Philosophy of Biology* (Oxford University Press, New York, 2018).
- [27] B. J. West, The fractal tapestry of life: II Entailment of fractional oncology by physiology networks, *Front. Netw. Physiol.* **2**, 845495 (2022).
- [28] A. G. Cherstvy, A. V. Chechkin, and R. Metzler, Anomalous diffusion and ergodicity breaking in heterogeneous diffusion processes, *New J. Phys.* **15**, 083039 (2013).
- [29] A. G. Cherstvy and R. Metzler, Nonergodicity, fluctuations, and criticality in heterogeneous diffusion processes, *Phys. Rev. E* **90**, 012134 (2014).
- [30] E. L. Hamaker, C. V. Dolan, and P. C. Molenaar, Statistical modeling of the individual: Rationale and application of multivariate stationary time series analysis, *Multivar. Behav. Res.* **40**, 207 (2005).
- [31] J.-H. Jeon, V. Tejedor, S. Burov, E. Barkai, C. Selhuber-Unkel, K. Berg-Sørensen, L. Oddershede, and R. Metzler, *In vivo* anomalous diffusion and weak ergodicity breaking of lipid granules, *Phys. Rev. Lett.* **106**, 048103 (2011).
- [32] J. Li, J. Xie, A. Godec, K. R. Weninger, C. Liu, J. C. Smith, and L. Hong, Non-ergodicity of a globular protein extending beyond its functional timescale, *Chem. Sci.* **13**, 9668 (2022).
- [33] R. Metzler, J.-H. Jeon, A. G. Cherstvy, and E. Barkai, Anomalous diffusion models and their properties: Non-stationarity, non-ergodicity, and ageing at the centenary of single particle tracking, *Phys. Chem. Chem. Phys.* **16**, 24128 (2014).
- [34] P. C. Molenaar, A manifesto on psychology as idiographic science: Bringing the person back into scientific psychology, this time forever, *Measurement* **2**, 201 (2004).
- [35] P. C. Molenaar, On the implications of the classical ergodic theorems: Analysis of developmental processes has to focus on intra-individual variation, *Dev. Psychobiol.* **50**, 60 (2008).
- [36] P. Molenaar, K. O. Sinclair, M. J. Rovine, N. Ram, and S. E. Corneal, Analyzing developmental processes on an individual level using nonstationary time series modeling, *Dev. Psychobiol.* **45**, 260 (2009).
- [37] P. C. Molenaar and C. G. Campbell, The new person-specific paradigm in psychology, *Curr. Dir. Psychol. Sci.* **18**, 112 (2009).
- [38] C. T. Kello, G. G. Anderson, J. G. Holden, and G. C. Van Orden, The pervasiveness of $1/f$ scaling in speech reflects the metastable basis of cognition, *Cognit. Sci.* **32**, 1217 (2008).
- [39] J. G. Holden, G. C. Van Orden, and M. T. Turvey, Dispersion of response times reveals cognitive dynamics, *Psychol. Rev.* **116**, 318 (2009).
- [40] B. B. Mandelbrot, Intermittent turbulence in self-similar cascades: Divergence of high moments and dimension of the carrier, *J. Fluid Mech.* **62**, 331 (1974).
- [41] D. Sornette, *Critical Phenomena in Natural Sciences: Chaos, Fractals, Selforganization and Disorder: Concepts and Tools* (Springer, New York, 2006).
- [42] A. Chhabra and R. V. Jensen, Direct determination of the $f(\alpha)$ singularity spectrum, *Phys. Rev. Lett.* **62**, 1327 (1989).
- [43] T. C. Halsey, M. H. Jensen, L. P. Kadanoff, I. Procaccia, and B. I. Shraiman, Fractal measures and their singularities: The characterization of strange sets, *Phys. Rev. A* **33**, 1141 (1986).
- [44] D. G. Kelty-Stephen and M. Mangalam, Additivity suppresses multifractal nonlinearity due to multiplicative cascade dynamics, *Physica A* **637**, 129573 (2024).
- [45] M. Mangalam and D. G. Kelty-Stephen, Multifractal perturbations to multiplicative cascades promote multifractal nonlinearity with asymmetric spectra, *Phys. Rev. E* **109**, 064212 (2024).
- [46] M. Mangalam, A. D. Likens, and D. G. Kelty-Stephen, Multifractal nonlinearity as a robust indicator of multiplicative cascade dynamics, [arXiv:2312.05653](https://arxiv.org/abs/2312.05653).
- [47] D. G. Kelty-Stephen and M. Mangalam, Fractal and multifractal descriptors restore ergodicity broken by non-Gaussianity in time series, *Chaos Solitons Fractals* **163**, 112568 (2022).
- [48] D. G. Kelty-Stephen and M. Mangalam, Multifractal descriptors ergodically characterize non-ergodic multiplicative cascade processes, *Physica A* **617**, 128651 (2023).
- [49] M. Mangalam and D. G. Kelty-Stephen, Point estimates, Simpson's paradox, and nonergodicity in biological sciences, *Neurosci. Biobehav. Rev.* **125**, 98 (2021).
- [50] M. Mangalam and D. G. Kelty-Stephen, Ergodic descriptors of non-ergodic stochastic processes, *J. R. Soc. Interface* **19**, 20220095 (2022).
- [51] M. Mangalam, R. Metzler, and D. G. Kelty-Stephen, Ergodic characterization of nonergodic anomalous diffusion processes, *Phys. Rev. Res.* **5**, 023144 (2023).
- [52] H. Seckler, R. Metzler, D. G. Kelty-Stephen, and M. Mangalam, Multifractal spectral features enhance classification of anomalous diffusion, *Phys. Rev. E* **109**, 044133 (2024).
- [53] M. P. Furmanek, M. Mangalam, D. G. Kelty-Stephen, and G. Juras, Postural constraints recruit shorter-timescale processes into the non-Gaussian cascade processes, *Neurosci. Lett.* **741**, 135508 (2021).
- [54] D. G. Kelty-Stephen, M. P. Furmanek, and M. Mangalam, Multifractality distinguishes reactive from proactive cascades in postural control, *Chaos Solitons Fractals* **142**, 110471 (2021).
- [55] M. Mangalam and D. G. Kelty-Stephen, Hypothetical control of postural sway, *J. R. Soc. Interface* **18**, 20200951 (2021).
- [56] M. Mangalam, I.-C. Lee, K. M. Newell, and D. G. Kelty-Stephen, Visual effort moderates postural cascade dynamics, *Neurosci. Lett.* **742**, 135511 (2021).
- [57] O. Kardan, K. C. Adam, I. Mance, N. W. Churchill, E. K. Vogel, and M. G. Berman, Distinguishing cognitive effort and working memory load using scale-invariance and alpha suppression in EEG, *NeuroImage* **211**, 116622 (2020).
- [58] O. Kardan, A. J. Stier, E. A. Layden, K. W. Choe, M. Lyu, X. Zhang, S. L. Beilock, M. D. Rosenberg, and M. G. Berman, Improvements in task performance after practice are associated with scale-free dynamics of brain activity, *Netw. Neurosci.* **7**, 1129 (2023).
- [59] J. R. Anastas, D. G. Kelty-Stephen, and J. A. Dixon, Executive function as an interaction-dominant process, *Ecol. Psychol.* **26**, 262 (2014).

- [60] J. A. Dixon, J. G. Holden, D. Mirman, and D. G. Stephen, Multifractal dynamics in the emergence of cognitive structure, *Topics Cogn. Sci.* **4**, 51 (2012).
- [61] D. G. Stephen, J. R. Anastas, and J. A. Dixon, Scaling in cognitive performance reflects multiplicative multifractal cascade dynamics, *Front. Physiol.* **3**, 102 (2012).
- [62] C. A. Bell, N. S. Carver, J. A. Zbaracki, and D. G. Kelty-Stephen, Non-linear amplification of variability through interaction across scales supports greater accuracy in manual aiming: Evidence from a multifractal analysis with comparisons to linear surrogates in the Fitts task, *Front. Physiol.* **10**, 998 (2019).
- [63] L. Bloomfield, E. Lane, M. Mangalam, and D. G. Kelty-Stephen, Perceiving and remembering speech depend on multifractal nonlinearity in movements producing and exploring speech, *J. R. Soc. Interface* **18**, 20210272 (2021).
- [64] N. Jacobson, Q. Berleman-Paul, M. Mangalam, D. G. Kelty-Stephen, and C. Ralston, Multifractality in postural sway supports quiet eye training in aiming tasks: A study of golf putting, *Hum. Mov. Sci.* **76**, 102752 (2021).
- [65] D. G. Kelty-Stephen, I. C. Lee, N. S. Carver, K. M. Newell, and M. Mangalam, Multifractal roots of suprapostural dexterity, *Hum. Mov. Sci.* **76**, 102771 (2021).
- [66] D. G. Kelty-Stephen and J. A. Dixon, Interwoven fluctuations during intermodal perception: Fractality in head sway supports the use of visual feedback in haptic perceptual judgments by manual wielding, *J. Exp. Psychol. Hum. Percept. Perform.* **40**, 2289 (2014).
- [67] M. Mangalam and D. G. Kelty-Stephen, Multiplicative-cascade dynamics supports whole-body coordination for perception via effortful touch, *Hum. Mov. Sci.* **70**, 102595 (2020).
- [68] Z. Palatinus, D. G. Kelty-Stephen, J. Kinsella-Shaw, C. Carello, and M. T. Turvey, Haptic perceptual intent in quiet standing affects multifractal scaling of postural fluctuation, *J. Exp. Psychol. Hum. Percept. Perform.* **40**, 1808 (2014).
- [69] N. S. Carver, D. Bojovic, and D. G. Kelty-Stephen, Multifractal foundations of visually-guided aiming and adaptation to prismatic perturbation, *Hum. Mov. Sci.* **55**, 61 (2017).
- [70] M. Mangalam, N. S. Carver, and D. G. Kelty-Stephen, Global broadcasting of local fractal fluctuations in a bodywide distributed system supports perception via effortful touch, *Chaos, Solitons Fractals* **135**, 109740 (2020).
- [71] M. Mangalam, N. S. Carver, and D. G. Kelty-Stephen, Multifractal signatures of perceptual processing on anatomical sleeves of the human body, *J. R. Soc. Interface* **17**, 20200328 (2020).
- [72] M. Mangalam, D. G. Kelty-Stephen, K. Kiyono, and N. Stergiou, Spatial variability and directional shifts in postural control in Parkinson's disease, *Clin. Parkinsonism Relat. Disord.* **10**, 100249 (2024).
- [73] M. Mangalam, D. G. Kelty-Stephen, I. Seleznev, A. Popov, A. D. Likens, K. Kiyono, and N. Stergiou, Older adults and individuals with Parkinson's disease control posture along suborthogonal directions that deviate from the traditional anteroposterior and mediolateral directions, *Sci. Rep.* **14**, 4117 (2024).
- [74] D. Kelty-Stephen, O. D. Similton, E. Rabinowitz, and M. Allen, Multifractal auditory stimulation promotes the effect of multifractal torso sway on spatial perception: Evidence from distance perception by blindwalking, *Ecol. Psychol.* **35**, 136 (2023).
- [75] M. Mangalam, D. G. Kelty-Stephen, J. H. Sommerfeld, N. Stergiou, and A. D. Likens, Temporal organization of stride-to-stride variations contradicts predictive models for sensorimotor control of footfalls during walking, *PLoS ONE* **18**, e0290324 (2023).
- [76] D. G. Stephen and J. A. Dixon, Strong anticipation: Multifractal cascade dynamics modulate scaling in synchronization behaviors, *Chaos Solitons Fractals* **44**, 160 (2011).
- [77] R. M. Ward and D. G. Kelty-Stephen, Bringing the nonlinearity of the movement system to gestural theories of language use: Multifractal structure of spoken english supports the compensation for coarticulation in human speech perception, *Front. Physiol.* **9**, 1152 (2018).
- [78] J. Suckling, A. M. Wink, F. A. Bernard, A. Barnes, and E. Bullmore, Endogenous multifractal brain dynamics are modulated by age, cholinergic blockade and cognitive performance, *J. Neurosci. Methods* **174**, 292 (2008).
- [79] G. Gaurav, R. S. Anand, and V. Kumar, EEG based cognitive task classification using multifractal detrended fluctuation analysis, *Cognit. Neurodyn.* **15**, 999 (2021).
- [80] A. Humeau, F. Chapeau-Blondeau, D. Rousseau, P. Rousseau, W. Trzepizur, and P. Abraham, Multifractality, sample entropy, and wavelet analyses for age-related changes in the peripheral cardiovascular system: Preliminary results, *Med. Phys.* **35**, 717 (2008).
- [81] B. J. West, M. Latka, M. Glaubic-Latka, and D. Latka, Multifractality of cerebral blood flow, *Physica A* **318**, 453 (2003).
- [82] S. Dutta, D. Ghosh, and S. Chatterjee, Multifractal detrended fluctuation analysis of human gait diseases, *Front. Physiol.* **4**, 274 (2013).
- [83] S. Dutta, D. Ghosh, and S. Chatterjee, Multifractal detrended cross correlation analysis of neuro-degenerative diseases—an in depth study, *Physica A* **491**, 188 (2018).
- [84] C. J. Morales and E. D. Kolaczyk, Wavelet-based multifractal analysis of human balance, *Ann. Biomed. Eng.* **30**, 588 (2002).
- [85] S. Lahmiri, A wavelet leaders model with multiscale entropy measures for diagnosing arrhythmia and congestive heart failure, *Healthcare Anal.* **3**, 100171 (2023).
- [86] M. Meyer and O. Stiedl, Self-affine fractal variability of human heartbeat interval dynamics in health and disease, *Eur. J. Appl. Physiol.* **90**, 305 (2003).
- [87] P. C. Ivanov, L. A. N. Amaral, A. L. Goldberger, S. Havlin, M. G. Rosenblum, Z. R. Struzik, and H. E. Stanley, Multifractality in human heartbeat dynamics, *Nature (London)* **399**, 461 (1999).
- [88] J. Wang, X. Ning, and Y. Chen, Multifractal analysis of electronic cardiogram taken from healthy and unhealthy adult subjects, *Physica A* **323**, 561 (2003).
- [89] C. F. Reyes-Manzano, C. Lerma, J. C. Echeverría, M. Martínez-Lavin, L. A. Martínez-Martínez, O. Infante, and L. Guzmán-Vargas, Multifractal analysis reveals decreased non-linearity and stronger anticorrelations in heart period fluctuations of fibromyalgia patients, *Front. Physiol.* **9**, 1118 (2018).
- [90] S. Chatterjee, S. Singha Roy, R. Bose, and S. Pratiher, Feature extraction from multifractal spectrum of electromyograms for diagnosis of neuromuscular disorders, *IET Sci. Meas. Technol.* **14**, 817 (2020).

- [91] T. Zorick, J. Landers, A. Leuchter, and M. A. Mandelkern, EEG multifractal analysis correlates with cognitive testing scores and clinical staging in mild cognitive impairment, *J. Clin. Neurosci.* **76**, 195 (2020).
- [92] F. Wang, H. Wang, X. Zhou, and R. Fu, A driving fatigue feature detection method based on multifractal theory, *IEEE Sens. J.* **22**, 19046 (2022).
- [93] J. Vasiljevic, B. Reljin, J. Sopta, V. Mijucic, G. Tulic, and I. Reljin, Application of multifractal analysis on microscopic images in the classification of metastatic bone disease, *Biomed. Microdevices* **14**, 541 (2012).
- [94] R. Bose, S. Pratiher, and S. Chatterjee, Detection of epileptic seizure employing a novel set of features extracted from multifractal spectrum of electroencephalogram signals, *IET Signal Process.* **13**, 157 (2019).
- [95] A. V. Perez-Sanchez, J. P. Amezcua-Sanchez, M. Valtierra-Rodriguez, and H. Adeli, A new epileptic seizure prediction model based on maximal overlap discrete wavelet packet transform, homogeneity index, and machine learning using ECG signals, *Biomed. Signal Process. Control* **88**, 105659 (2024).
- [96] D. Sikdar, R. Roy, and M. Mahadevappa, Epilepsy and seizure characterisation by multifractal analysis of EEG subbands, *Biomed. Signal Process. Control* **41**, 264 (2018).
- [97] Y. Zhang, W. Zhou, and S. Yuan, Multifractal analysis and relevance vector machine-based automatic seizure detection in intracranial EEG, *Int. J. Neural Syst.* **25**, 1550020 (2015).
- [98] N. Brodu, F. Lotte, and A. Lécuyer, Exploring two novel features for EEG-based brain-computer interfaces: Multifractal cumulants and predictive complexity, *Neurocomputing* **79**, 87 (2012).
- [99] M. M. Abdelsalam and M. Zahran, A novel approach of diabetic retinopathy early detection based on multifractal geometry analysis for OCTA macular images using support vector machine, *IEEE Access* **9**, 22844 (2021).
- [100] Y. Ding, W. O. Ward, J. Duan, D. Auer, P. Gowland, and L. Bai, Retinal vasculature classification using novel multifractal features, *Phys. Med. Biol.* **60**, 8365 (2015).
- [101] M. Ando, S. Nobukawa, M. Kikuchi, and T. Takahashi, Identification of electroencephalogram signals in Alzheimer's disease by multifractal and multiscale entropy analysis, *Front. Neurosci.* **15**, 667614 (2021).
- [102] Y. M. Elgammal, M. Zahran, and M. M. Abdelsalam, A new strategy for the early detection of alzheimer disease stages using multifractal geometry analysis based on K-nearest neighbor algorithm, *Sci. Rep.* **12**, 22381 (2022).
- [103] H. Ni, L. Zhou, X. Ning, and L. Wang, Exploring multifractal-based features for mild Alzheimer's disease classification, *Magn. Reson. Med.* **76**, 259 (2016).
- [104] C. Atupelage, H. Nagahashi, M. Yamaguchi, T. Abe, A. Hashiguchi, and M. Sakamoto, Computational grading of hepatocellular carcinoma using multifractal feature description, *Comput. Med. Imaging Graphics* **37**, 61 (2013).
- [105] P. Karthick, D. M. Ghosh, and S. Ramakrishnan, Surface electromyography based muscle fatigue detection using high-resolution time-frequency methods and machine learning algorithms, *Comput. Methods Programs Biomed.* **154**, 45 (2018).
- [106] K. Marri and R. Swaminathan, Classification of muscle fatigue in dynamic contraction using surface electromyography signals and multifractal singularity spectral analysis, *J. Dyn. Syst. Meas. Control* **138**, 111008 (2016).
- [107] S. Lahmiri, Glioma detection based on multi-fractal features of segmented brain MRI by particle swarm optimization techniques, *Biomed. Signal Process. Control* **31**, 148 (2017).
- [108] M. A. Mohammed, B. Al-Khateeb, A. N. Rashid, D. A. Ibrahim, M. K. Abd Ghani, and S. A. Mostafa, Neural network and multi-fractal dimension features for breast cancer classification from ultrasound images, *Comput. Electr. Eng.* **70**, 871 (2018).
- [109] P. Abry, H. Wendt, and S. Jaffard, When Van Gogh meets Mandelbrot: Multifractal classification of painting's texture, *Signal Process.* **93**, 554 (2013).
- [110] M. Bigerelle and A. Iost, Fractal dimension and classification of music, *Chaos Solitons Fractals* **11**, 2179 (2000).
- [111] Z.-Y. Su and T. Wu, Multifractal analyses of music sequences, *Physica D* **221**, 188 (2006).
- [112] T. C. Roeske, D. Kely-Stephen, and S. Wallot, Multifractal analysis reveals music-like dynamic structure in songbird rhythms, *Sci. Rep.* **8**, 4570 (2018).
- [113] S. Nag, M. Basu, S. Sanyal, A. Banerjee, and D. Ghosh, On the application of deep learning and multifractal techniques to classify emotions and instruments using Indian classical music, *Physica A* **597**, 127261 (2022).
- [114] N. Reljin and D. Pokrajac, Music performers classification by using multifractal features: A case study, *Arch. Acoust.* **42**, 223 (2017).
- [115] L. Parisi, N. RaviChandran, and M. L. Manaog, Feature-driven machine learning to improve early diagnosis of Parkinson's disease, *Expert Syst. Appl.* **110**, 182 (2018).
- [116] R. Prashanth, S. D. Roy, P. K. Mandal, and S. Ghosh, High-accuracy detection of early Parkinson's disease through multimodal features and machine learning, *Int. J. Med. Inf.* **90**, 13 (2016).
- [117] A. Suppa, G. Costantini, F. Ascì, P. Di Leo, M. S. Al-Wardat, G. Di Lazzaro, S. Scalise, A. Pisani, and G. Saggio, Voice in Parkinson's disease: A machine learning study, *Front. Neurol.* **13**, 831428 (2022).
- [118] W. Wang, J. Lee, F. Harrou, and Y. Sun, Early detection of Parkinson's disease using deep learning and machine learning, *IEEE Access* **8**, 147635 (2020).
- [119] K. L. Chou, M. Stacy, T. Simuni, J. Miyasaki, W. H. Oertel, K. Sethi, H. H. Fernandez, and F. Stocchi, The spectrum of "off" in Parkinson's disease: What have we learned over 40 years? *Parkinsonism Relat. Disord.* **51**, 9 (2018).
- [120] A. Rajput, H. Sitte, A. Rajput, M. Fenton, C. Pifl, and O. Hornykiewicz, Globus pallidus dopamine and Parkinson motor subtypes: Clinical and brain biochemical correlation, *Neurology* **70**, 1403 (2008).
- [121] S. Sveinbjornsdottir, The clinical symptoms of Parkinson's disease, *J. Neurochem.* **139**, 318 (2016).
- [122] M. T. Turvey and S. T. Fonseca, The medium of haptic perception: A tensegrity hypothesis, *J. Mot. Behav.* **46**, 143 (2014).
- [123] B. B. Mandelbrot, *The Fractal Geometry of Nature* (WH Freeman, New York, 1982), Vol. 1.
- [124] B. B. Mandelbrot, *Fractals and Scaling in Finance: Discontinuity, Concentration, Risk* (Springer, New York, 2013).
- [125] M. Zamir, Critique of the test of multifractality as applied to biological data, *J. Theor. Biol.* **225**, 407 (2003).

- [126] E. A. F. E. Ihlen, Introduction to multifractal detrended fluctuation analysis in Matlab, *Front. Physiol.* **3**, 141 (2012).
- [127] T. Schreiber and A. Schmitz, Improved surrogate data for nonlinearity tests, *Phys. Rev. Lett.* **77**, 635 (1996).
- [128] R. Bro and A. K. Smilde, Principal component analysis, *Anal. Methods* **6**, 2812 (2014).
- [129] S. Lloyd, Least squares quantization in PCM, *IEEE Trans. Inf. Theory* **28**, 129 (1982).
- [130] E. Alpaydin, *Introduction to Machine Learning*, (MIT Press, Cambridge, MA, 2020).
- [131] L. V. Fausett, *Fundamentals of Neural Networks: Architectures, Algorithms and Applications* (Prentice Hall, Hoboken, NJ, 1994).
- [132] Z. Zhang and M. Sabuncu, Generalized cross entropy loss for training deep neural networks with noisy labels, *Advances in Neural Information Processing Systems* (Curran Associates, Inc., Red Hook, NY, 2018), Vol. 31.
- [133] L. Bottou, Large-scale machine learning with stochastic gradient descent, in *Proceedings of COMPSTAT'2010: 19th International Conference on Computational Statistics*, Paris, August 22–27, 2010 Keynote, Invited and Contributed Papers (Springer, Berlin, 2010), pp. 177–186.
- [134] D. P. Kingma and J. Ba, Adam: A method for stochastic optimization, [arXiv:1412.6980](https://arxiv.org/abs/1412.6980).
- [135] W. J. Maddox, P. Izmailov, T. Garipov, D. P. Vetrov, and A. G. Wilson, A simple baseline for bayesian uncertainty in deep learning, *Advances in Neural Information Processing Systems* (Curran Associates, Inc., Red Hook, NY, 2018), Vol. 32.
- [136] R. H. Hahnloser, R. Sarpeshkar, M. A. Mahowald, R. J. Douglas, and H. S. Seung, Digital selection and analogue amplification coexist in a cortex-inspired silicon circuit, *Nature (London)* **405**, 947 (2000).
- [137] B. Gao and L. Pavel, On the properties of the softmax function with application in game theory and reinforcement learning, [arXiv:1704.00805](https://arxiv.org/abs/1704.00805).
- [138] H. Seckler, J. Szwabinski, and R. Metzler, Machine-learning solutions for the analysis of single-particle diffusion trajectories, *J. Phys. Chem. Lett.* **14**, 7910 (2023).
- [139] D. G. Kelty-Stephen, K. Palatinus, E. Saltzman, and J. A. Dixon, A tutorial on multifractality, cascades, and interactivity for empirical time series in ecological science, *Ecol. Psychol.* **25**, 1 (2013).
- [140] D. G. Kelty-Stephen, E. Lane, and M. Mangalam, Multifractal test for nonlinearity of interactions across scales in time series, *Behav. Res. Methods* **55**, 2249 (2023).
- [141] M. Gjoreski, A. Gradišek, B. Budna, M. Gams, and G. Poglajen, Machine learning and end-to-end deep learning for the detection of chronic heart failure from heart sounds, *IEEE Access* **8**, 20313 (2020).
- [142] A. Jovic, K. Brkic, and G. Krstacic, Detection of congestive heart failure from short-term heart rate variability segments using hybrid feature selection approach, *Biomed. Signal Process. Control* **53**, 101583 (2019).
- [143] L. Wang, W. Zhou, Q. Chang, J. Chen, and X. Zhou, Deep ensemble detection of congestive heart failure using short-term RR intervals, *IEEE Access* **7**, 69559 (2019).
- [144] J. R. de Miras, A. J. Ibáñez-Molina, M. F. Soriano, and S. Iglesias-Parro, Schizophrenia classification using machine learning on resting state EEG signal, *Biomed. Signal Process. Control* **79**, 104233 (2023).
- [145] J. K. Johannesen, J. Bi, R. Jiang, J. G. Kenney, and C.-M. A. Chen, Machine learning identification of EEG features predicting working memory performance in schizophrenia and healthy adults, *Neuropsychiatr. Electrophysiol.* **2**, 3 (2016).
- [146] M. A. Vázquez, A. Maghsoudi, and I. P. Mariño, An interpretable machine learning method for the detection of schizophrenia using EEG signals, *Front. Syst. Neurosci.* **15**, 652662 (2021).
- [147] S. Drożdż and P. Oświecimka, Detecting and interpreting distortions in hierarchical organization of complex time series, *Phys. Rev. E* **91**, 030902(R) (2015).
- [148] T. J. Wilson, M. Mangalam, N. Stergiou, and A. D. Likens, Multifractality in stride-to-stride variations reveals that walking involves more movement tuning and adjusting than running, *Front. Netw. Physiol.* **3**, 1294545 (2023).
- [149] S. Kian-Bostanabad and M.-R. Azghani, The relationship between RMS electromyography and thickness change in the skeletal muscles, *Med. Eng. Phys.* **43**, 92 (2017).
- [150] J. Vink, M. Westover, A. Pascual-Leone, and M. Shafi, EEG functional connectivity predicts propagation of TMS-evoked potentials, *Brain Stimul.* **10**, 516 (2017).
- [151] J. J. Vink, D. C. Klooster, R. A. Ozdemir, M. B. Westover, A. Pascual-Leone, and M. M. Shafi, EEG functional connectivity is a weak predictor of causal brain interactions, *Brain Topogr.* **33**, 221 (2020).
- [152] C. R. Booth, H. L. Brown, E. G. Eason, S. Wallot, and D. G. Kelty-Stephen, Expectations on hierarchical scales of discourse: Multifractality predicts both short-and long-range effects of violating gender expectations in text reading, *Discourse Process.* **55**, 12 (2018).
- [153] M. Mangalam, R. Chen, T. R. McHugh, T. Singh, and D. G. Kelty-Stephen, Bodywide fluctuations support manual exploration: Fractal fluctuations in posture predict perception of heaviness and length via effortful touch by the hand, *Hum. Mov. Sci.* **69**, 102543 (2020).
- [154] S. Wallot and D. G. Kelty-Stephen, Interaction-dominant causation in mind and brain, and its implication for questions of generalization and replication, *Mines Mach.* **28**, 353 (2018).
- [155] D. G. Kelty-Stephen and M. Mangalam, Turing's cascade instability supports the coordination of the mind, brain, and behavior, *Neurosci. Biobehav. Rev.* **141**, 104810 (2022).
- [156] H. Seckler and R. Metzler, Bayesian deep learning for error estimation in the analysis of anomalous diffusion, *Nat. Commun.* **13**, 6717 (2022).
- [157] X. Xiao, H. Chen, and P. Bogdan, Deciphering the generating rules and functionalities of complex networks, *Sci. Rep.* **11**, 22964 (2021).
- [158] N. Bernstein, *The Co-ordination and Regulation of Movements*, (Pergamon, Oxford, 1996).
- [159] N. A. Bernstein, *Dexterity and Its Development* (Lawrence Erlbaum, Mahwah, NJ, 1996).
- [160] H. H. Pattee, The physics of symbols: Bridging the epistemic cut, *Biosystems* **60**, 5 (2001).
- [161] H. H. Pattee, Laws, constraints, and the modeling relationship and interpretations, *Chem. Biodivers.* **4**, 2272 (2007).
- [162] H. H. Pattee, The physical basis and origin of hierarchical control, in *Laws, Language and Life: Howard Pattee's Classic Papers on the Physics of Symbols with Contemporary Commentary*, edited by H. H. Pattee and J. Rączaszek-Leonardi (Springer, Dordrecht, 2012), pp. 91–110.

- [163] H. H. Pattee, Epistemic, evolutionary, and physical conditions for biological information, *Biosemiotics* **6**, 9 (2013).
- [164] V. L. Profeta and M. T. Turvey, Bernstein's levels of movement construction: A contemporary perspective, *Hum. Mov. Sci.* **57**, 111 (2018).
- [165] M. L. Latash, The Bernstein problem: How does the central nervous system make its choices, in *Dexterity and Its Development* (Psychology Press, New York, 1996), pp. 277–303.
- [166] M. L. Latash, *Synergy* (Oxford University Press, New York, 2008).
- [167] M. L. Latash, The bliss (not the problem) of motor abundance (not redundancy), *Exp. Brain Res.* **217**, 1 (2012).
- [168] M. L. Latash, On primitives in motor control, *Motor Control* **24**, 318 (2020).
- [169] M. L. Latash, What do synergies do at Bernstein's level of synergies? in *Bernstein's Construction of Movements* (Routledge, New York, 2020), pp. 344–352.
- [170] M. L. Latash and V. L. Talis, Bernstein's philosophy of time: An unknown manuscript by Nikolai Bernstein (1949), *Motor Control* **25**, 315 (2021).
- [171] M. L. Latash, One more time about motor (and non-motor) synergies, *Exp. Brain Res.* **239**, 2951 (2021).
- [172] S. Reschektko and M. L. Latash, Stability of hand force production. II. Ascending and descending synergies, *J. Neurophysiol.* **120**, 1045 (2018).
- [173] M. J. Hove, K. Suzuki, H. Uchitomi, S. Orimo, and Y. Miyake, Interactive rhythmic auditory stimulation reinstates natural $1/f$ timing in gait of Parkinson's patients, *PLoS ONE* **7**, e32600 (2012).
- [174] D. Nozaki, J. J. Collins, and Y. Yamamoto, Mechanism of stochastic resonance enhancement in neuronal models driven by $1/f$ noise, *Phys. Rev. E* **60**, 4637 (1999).
- [175] G. C. Peng, M. Alber, A. Buganza Tepole, W. R. Cannon, S. De, S. Dura-Bernal, K. Garikipati, G. Karniadakis, W. W. Lytton, P. Perdikaris *et al.*, Multiscale modeling meets machine learning: What can we learn? *Arch. Comput. Methods Eng.* **28**, 1017 (2021).
- [176] M. Mangalam, A. Sadri, J. Hayano, E. Watanabe, K. Kiyono, and D. G. Kelty-Stephen, Multifractal foundations of biomarker discovery for heart disease and stroke, *Sci. Rep.* **13**, 18316 (2023).
- [177] H. Stanley, L. N. Amaral, A. Goldberger, S. Havlin, P. C. Ivanov, and C.-K. Peng, Statistical physics and physiology: Monofractal and multifractal approaches, *Physica A* **270**, 309 (1999).
- [178] L. G. S. França, J. G. V. Miranda, M. Leite, N. K. Sharma, M. C. Walker, L. Lemieux, and Y. Wang, Fractal and multifractal properties of electrographic recordings of human brain activity: Toward its use as a signal feature for machine learning in clinical applications, *Front. Physiol.* **9**, 1767 (2018).
- [179] S. M. Shekatkar, Y. Kotriwar, K. Harikrishnan, and G. Ambika, Detecting abnormality in heart dynamics from multifractal analysis of ECG signals, *Sci. Rep.* **7**, 15127 (2017).
- [180] M. Mangalam, I. Seleznev, A. Popov, E. Kolosova, D. G. Kelty-Stephen, and K. Kiyono, Postural control in gymnasts: Anisotropic fractal scaling reveals proprioceptive reintegration in vestibular perturbation, *Front. Physiol.* **4**, 1393171 (2024).
- [181] W. Rahman, S. Lee, M. S. Islam, V. N. Antony, H. Ratnu, M. R. Ali, A. A. Mamun, E. Wagner, S. Jensen-Roberts, E. Waddell *et al.*, Detecting Parkinson disease using a web-based speech task: Observational study, *J. Med. Internet Res.* **23**, e26305 (2021).
- [182] K. Sechidis, R. Fusaroli, J. R. Orozco-Arroyave, D. Wolf, and Y.-P. Zhang, A machine learning perspective on the emotional content of Parkinsonian speech, *Artif. Intell. Med.* **115**, 102061 (2021).
- [183] A. Tsanas, M. A. Little, and L. O. Ramig, Remote assessment of Parkinson's disease symptom severity using the simulated cellular mobile telephone network, *IEEE Access* **9**, 11024 (2021).
- [184] N. A. Kuznetsov and S. Wallot, Effects of accuracy feedback on fractal characteristics of time estimation, *Front. Integr. Neurosci.* **5**, 62 (2011).
- [185] E. A. Ihlen and B. Vereijken, Multifractal formalisms of human behavior, *Hum. Mov. Sci.* **32**, 633 (2013).
- [186] M. Raissi, P. Perdikaris, and G. E. Karniadakis, Physics-informed neural networks: A deep learning framework for solving forward and inverse problems involving nonlinear partial differential equations, *J. Comput. Phys.* **378**, 686 (2019).
- [187] A. L. Goldberger, D. R. Rigney, and B. J. West, Chaos and fractals in human physiology, *Sci. Am.* **262**(2), 42 (1990).
- [188] S. Lovejoy and D. Schertzer, *The Weather and Climate: Emergent Laws and Multifractal Cascades* (Cambridge University Press, Cambridge, MA, 2018).
- [189] T. Sauer, J. A. Yorke, and M. Casdagli, Embedology, *J. Stat. Phys.* **65**, 579 (1991).
- [190] R. C. Deo, Machine learning in medicine, *Circulation* **132**, 1920 (2015).
- [191] A. K. Feeny, M. K. Chung, A. Madabhushi, Z. I. Attia, M. Cikes, M. Firouznia, P. A. Friedman, M. M. Kalscheur, S. Kapa, S. M. Narayan *et al.*, Artificial intelligence and machine learning in arrhythmias and cardiac electrophysiology, *Circ. Arrhythm. Electrophysiol.* **13**, e007952 (2020).
- [192] A. Madabhushi and G. Lee, Image analysis and machine learning in digital pathology: Challenges and opportunities, *Med. Image Anal.* **33**, 170 (2016).
- [193] J. H. Thrall, X. Li, Q. Li, C. Cruz, S. Do, K. Dreyer, and J. Brink, Artificial intelligence and machine learning in radiology: Opportunities, challenges, pitfalls, and criteria for success, *J. Am. Coll. Radiol.* **15**, 504 (2018).
- [194] S. Wang and R. M. Summers, Machine learning and radiology, *Med. Image Anal.* **16**, 933 (2012).
- [195] B. B. Mandelbrot, An introduction to multifractal distribution functions, in *Random Fluctuations and Pattern Growth: Experiments and Models* (Springer, New York, 1988), pp. 279–291.
- [196] B. B. Mandelbrot, A class of multinomial multifractal measures with negative (latent) values for the "dimension" $f(\alpha)$, in *Fractals' Physical Origin and Properties* (Springer, New York, 1989), p. 3.